The Astrophysical Journal Supplement Series, 155:149–165, 2004 November

A CATALOG OF CH_3OH 7_0–6_1 A^+ MASER SOURCES IN MASSIVE STAR-FORMING REGIONS

Stan Kurtz
Centro de Radioastronomía y Astrofísica, Universidad Nacional Autónoma de México, Apartado Postal 3-72, Morelia 58089, México

Peter Hofner
Physics Department, New Mexico Institute of Mining and Technology, Socorro, NM 87801; and National Radio Astronomy Observatory, P.O. Box O, Socorro, NM 87801

and

Carlos Vargas Álvarez[1]
Physics Department, University of Puerto Rico at Mayagüez, Mayagüez, PR 00680
Received 2004 January 7; accepted 2004 June 30

ABSTRACT

We present a Very Large Array survey of 44 massive star-forming regions in the 44 GHz 7_0–6_1 A^+ methanol transition; 37 fields showed maser emission. Thirty-one sources were also observed in the 23 GHz 9_2–10_1 A^+ methanol line; two fields showed maser emission. Although the 44 GHz line is a class I maser, we find a large number of these masers in relatively close association with H II regions and water masers. Several sources show strong evidence for a correlation between 44 GHz masers and shocked molecular gas, supporting the interpretation that molecular outflows may give rise to class I maser emission. We provide maser positions with arcsecond accuracy that not only locate the masers with respect to other star formation phenomena, but also provide, for the stronger masers, phase referencing sources that can be used to calibrate future 7 mm (44 GHz) observations of these regions.

Subject headings: catalogs — H II regions — ISM: molecules — masers — stars: early-type — stars: formation

Online material: machine-readable table

1. INTRODUCTION

The massive star formation process presents a number of physical phenomena including hot molecular cores (HMC), molecular outflows, ultracompact (UC) H II regions, and maser emission from various molecular species. The physical relationship between these phenomena is not always clear, nor is their order of appearance during the star formation process. Several relevant reviews are Garay & Lizano (1999), Evans (1999), and Churchwell (2002). High angular resolution observations of massive star-forming regions, tracing both ionized and molecular gas, are essential to determine the relationship between these phenomena and the role that each one plays in the massive star formation process.

Interferometric studies of massive star formation at *Q* band (7 mm or 40–50 GHz) are often hampered by the lack of adequate phase calibrators. The number of suitable calibrator sources drops rapidly with increasing frequency and the lack of nearby calibrators is a significant problem for 7 mm observations. A cross-calibration technique using maser sources described by Reid & Menten (1990) has been used very effectively at 1.3 cm with water masers (e.g., Torrelles et al. 1997). To extend the same technique to 7 mm—a wavelength at which continuum dust emission may be feasible to detect—requires a masing transition in the 40–50 GHz band. A suitable maser line is provided by the CH_3OH 7_0–6_1 A^+ transition at 44 GHz.

To provide precise information on the occurrence and location of methanol masers with respect to other massive star formation phenomena, and to search for strong 44 GHz masers that can be utilized in the maser cross-calibration procedure, we undertook a survey of methanol maser emission. In this paper we present the data obtained from this survey. In § 2 we describe the observational program. In § 3 we present the results in tabular form and provide a brief discussion and images for selected sources. In § 4 we discuss some of the astronomical implications of the results and in § 5 we reiterate the more important conclusions.

2. OBSERVATIONS

2.1. *Source Selection*

Several criteria were used to select the 44 sources observed in this survey. One of our foremost goals was to identify cross-calibration maser sources to use in interferometric *Q*-band observations of galactic star formation regions. Hence, many well-known massive star formation sites were included. In addition, because there has been considerable conjecture concerning the evolutionary stage at which methanol masers occur (see the review of Garay & Lizano 1999), we included both extremely young massive star formation regions, which have not yet developed an UC H II region, along with more evolved massive star formation regions, which have formed UC H II regions. The former category is typified by the Molinari sample (Molinari et al. 1996, 1998, 2000). This sample was developed to locate massive protostellar objects by successively applying various selection criteria designed to eliminate more evolved, high-mass objects (see Fig. 1 of Molinari et al. 2000). The Molinari sources are prime candidates for massive protostars, and we have searched a significant fraction of them for 44 GHz methanol maser emission. The latter category, of more evolved sources, we represent in our sample by including compact and UC H II regions with 44 GHz single-dish maser detections

[1] Currently at the Department of Astronomy, San Diego State University, San Diego, CA 92182-1221.

TABLE 1
SUMMARY OF OBSERVATIONS

Observation Date	VLA Configuration	Frequency (GHz)	Number of Sources[a]
1997 Sep 15.....	C	44, 23	16
1999 Mar 23.....	D	44, 23	15
2000 Sep 25[b].....	D	44	14

[a] Several sources were observed on more than one date; a total of 44 distinct sources were observed, including the 2001 November 30 observations.
[b] Two sources, GGD27 (HH 80–81) and Mol 138, were observed at 44 GHz during unrelated observations on 2001 November 30 with 20 antennas in the D array. We include the data here but do not report a fourth, dedicated observing run.

reported by Bachiller et al. (1990), Haschick et al. (1990), and Slysh et al. (1994).

2.2. *Radio Observations and Data Reduction*

Three observing runs were made, using the Very Large Array (VLA) of the NRAO.[2] An overview of the observations is presented in Table 1. At the time of the 1997 and 1999 observations, only 13 *Q*-band receivers were available at the VLA. In order to fully utilize the 27 element array, we simultaneously observed the CH_3OH 7_0–6_1 A^+ ($\nu_0 = 44.069430$ GHz) transition in the *Q*-band subarray and the CH_3OH 9_2–10_1 A^+ ($\nu_0 = 23.121024$ GHz) transition in the non–*Q*-band subarray. At the time of the 2000 observations, 18 antennas were equipped with *Q*-band receivers and only the 44 GHz transition was observed. In Tables 2, 3, and 4 we list the sources observed, along with the central bandpass velocity, the synthesized beam size, and the channel rms noise.

For all observations a 3.125 MHz bandwidth was used and only the right circular polarization was measured. After online Hanning smoothing the final spectra consist of 127 channels of width 24.414 kHz. For the 44 GHz line this correlator setup provides a velocity resolution of 0.17 km s^{-1} and velocity coverage of 21 km s^{-1}. The same correlator setup was used for the 23 GHz line, providing a resolution and coverage of 0.32 and 40 km s^{-1}, respectively.

Observations were made in a mixture of fast-switching mode and conventional calibrator-source-calibrator scans, according to the availability of a nearby calibrator. Referenced pointing was performed approximately once per hour or whenever switching to a substantially different region of the sky. No bandpass calibration was performed. Typical on-source integration times were 10 minutes.

A number of problems, unique to each observing run, were encountered in the flux calibration of the data. These problems included insufficient signal on phase-stable timescales, elevation-dependent gain changes, and rapid time variation of some phase calibrator flux densities. We estimate that the absolute flux density calibration uncertainty of the three runs is about 25%, 20%, and 30%, respectively. The primary goal of these observations is to provide positional information for the masers; as such, these flux calibration uncertainties are acceptable for our purposes. We caution, however, that they are larger than normal for VLA observations, and the data presented here are not suitable for high-precision variability studies.

For a number of sources, continuum emission was detected along with the masers. Comparison of the peak continuum position with values published in the literature provides a check of our astrometric accuracy. We conservatively estimate that the positional uncertainties of the three observing runs are 0.″5, 0.″6, and 0.″5, respectively.

Following an initial external calibration of the data, all fields were imaged over an area slightly larger than the 1′ (44 GHz) or 2′ (23 GHz) primary beam; the resulting maps were then searched for maser emission. When maser emission was found, one of several different procedures was followed, depending on the circumstances. When possible, the strongest, most-isolated maser component was identified and the corresponding channel

[2] The National Radio Astronomy Observatory is operated by Associated Universities, Inc., under contract with the National Science Foundation.

TABLE 2
OBSERVED SOURCES: FIRST RUN

Source	Pointing Center		Central Velocity	Synthesized Beam[a]		Channel Map rms[a]	44 GHz Maser Detection
	α (B1950)	δ (B1950)	(km s^{-1})	(arcsec)	(deg)	(mJy $beam^{-1}$)	
S235	05 37 31.80	+35 40 18.0	−16.4	0.57 × 0.37	+89.7	60	Yes
S255	06 09 58.00	+18 01 13.0	+11.2	0.65 × 0.41	−71.7	95	Yes
NGC 6334F.....	17 17 32.20	−35 44 04.0	−6.1	1.17 × 0.30	+9.7	100	Yes[b]
G8.67−0.36.....	18 03 19.00	−21 37 59.0	+35.7	0.72 × 0.33	+6.5	75	Yes[b]
G10.62−0.38.....	18 07 30.50	−19 56 28.0	−4.0	0.69 × 0.35	+8.5	80	Yes
G12.89+0.49	18 08 56.40	−17 32 14.0	+30.0	0.68 × 0.34	+9.8	80	Yes
G11.94−0.62.....	18 11 04.40	−18 54 20.0	+35.8	0.77 × 0.37	+18.4	80	Yes
M17.....	18 17 31.00	−16 12 50.0	+18.9	0.68 × 0.38	+21.5	80	Yes[b]
G45.12+0.13	19 11 06.20	+10 48 26.0	+60.0	0.44 × 0.38	−14.6	100	No
W51 E1.....	19 21 26.20	+14 24 43.0	+52.0	0.44 × 0.41	−29.7	70	Yes
K3-50	19 59 50.10	+33 24 17.0	−20.0	0.96 × 0.37	+34.7	80	No
ON1.....	20 08 09.90	+31 22 42.0	+11.4	0.45 × 0.38	−62.2	60	Yes
ON2.....	20 19 52.00	+37 17 00.0	−2.0	0.47 × 0.36	−64.6	55	Yes
W75 N.....	20 36 50.40	+42 27 23.0	+8.9	0.95 × 0.36	+30.1	65	Yes
DR 21.....	20 37 14.00	+42 09 05.0	−3.8	0.50 × 0.37	−80.0	100	Yes
NGC 7538.....	23 11 36.70	+61 11 49.0	−57.4	0.96 × 0.44	+25.3	80	Yes[c]

NOTE.—Units of right ascension are hours, minutes, and seconds, and units of declination are degrees, arcminutes, and arcseconds.
[a] The beam and noise parameters are for the 44 GHz maps. The average 23 GHz beam was 1.″37 × 0.″96; the channel rms ranged from 70 to 130 mJy $beam^{-1}$.
[b] 44 GHz maser emission was clearly detected in this field, but we are not able to reliably determine its position. Only velocity information is provided in Table 5.
[c] A 23 GHz maser was also detected for NGC 7538; see Table 6.

TABLE 3
OBSERVED SOURCES: SECOND RUN

Source	Pointing Center		Central Velocity	Synthesized Beam[a]		Channel Map rms[a]	44 GHz Maser Detection
	α (B1950)	δ (B1950)	(km s^{-1})	(arcsec)	(deg)	(mJy beam^{-1})	
W3(OH)	02 23 17.30	+61 38 57.2	−46.0	3.09 × 1.56	+53.3	55	No[b]
G139.90+0.19	03 03 31.50	+58 19 21.0	−39.0	2.95 × 1.66	+58.1	55	No
G5.89−0.39	17 57 26.80	−24 03 56.0	+11.0	3.68 × 1.46	−15.6	60	Yes
G9.62+0.19	18 03 16.00	−20 32 00.0	+3.0	3.68 × 1.44	−19.5	60	Yes
G10.47+0.03	18 05 40.30	−19 52 20.0	+65.0	3.14 × 1.33	−7.7	75	Yes[c]
G12.21−0.10	18 09 44.00	−18 25 10.0	+24.0	2.93 × 1.43	−5.2	40	Yes
G19.62−0.23	18 24 50.30	−11 58 30.0	+41.0	2.61 × 1.53	−4.6	60	Yes
G29.96−0.02	18 43 27.00	−02 42 36.0	+98.0	4.18 × 1.89	−28.4	55	Yes
G31.41+0.31	18 44 59.00	−01 16 06.0	+98.0	2.21 × 1.36	+5.4	50	Yes[c]
G34.26+0.15	18 50 46.20	+01 11 12.0	+57.0	2.18 × 1.57	+7.6	55	Yes
G45.07+0.13	19 11 00.40	+10 45 43.0	+60.0	1.98 × 1.60	+7.0	45	Yes
G45.47+0.05	19 12 04.30	+11 04 11.0	+62.0	2.17 × 1.54	+5.3	55	Yes
W51 N	19 21 22.40	+14 25 16.0	+60.0	3.09 × 2.20	+26.5	65	Yes
20126+4104	20 12 41.00	+41 04 21.0	−4.0	1.81 × 1.48	−18.0	15	Yes
DR 21(OH)	20 37 14.00	+42 12 11.0	−5.0	1.89 × 1.51	−22.5	50	Yes

NOTE.—Units of right ascension are hours, minutes, and seconds, and units of declination are degrees, arcminutes, and arcseconds.
[a] The beam and noise parameters are for the 44 GHz maps. The average 23 GHz beam was 4.″31 × 3.″02; the channel rms ranged from 30 to 50 mJy beam^{-1}.
[b] A 23 GHz maser was detected in W3(OH); see Table 6.
[c] This source could not be imaged in the second run; it was reobserved in the third run.

was self-calibrated in phase only; this calibration was then applied to the other channels. In many cases, the resulting images were sufficiently close to the theoretical noise limit that no further self-calibration was done. In some cases, a second iteration, of phase and amplitude self-calibration was also made. For a number of sources—particularly in the first two observing runs when the smaller number of antennas resulted in relatively poor *uv* coverage—it was difficult to determine the absolute maser position to begin the self-calibration procedure. For some of these sources we detected continuum emission, and in those cases we were able to initiate self-calibration using a continuum map as the model. This allowed the masers to be located within the field, and the strongest component was then used for further iterations of self-calibration. In three cases we were not able to reliably determine the maser positions although maser emission was clearly present in the field. These sources are indicated in footnotes to the data tables.

After an acceptable calibration of the data was achieved, each data set was imaged and CLEANed interactively, with CLEAN boxes set around each maser. The resulting image cubes were inspected for additional, weaker masers, which, if found, were assigned appropriate CLEAN boxes. A final image cube was made with all masers assigned CLEAN boxes and CLEANing to a flux limit of twice the theoretical noise. The maser parameters (position, velocity, and integrated line flux) were determined from these cubes. The noise levels of the final data cubes are indicated in Tables 2–4. The worst-case 5 σ detection limit is 0.5 Jy, and the median 5 σ limit is

TABLE 4
OBSERVED SOURCES: THIRD RUN

Source	Pointing Center		Central Velocity	Synthesized Beam		Channel Map rms	44 GHz Maser Detection
	α (J2000)	δ (J2000)	(km s^{-1})	(arcsec)	(deg)	(mJy beam^{-1})	
S255	06 12 53.40	+18 00 23.0	+11.2	4.01 × 1.77	−66.3	55	Yes
G10.47+0.03	18 08 38.20	−19 51 49.0	+65.0	3.07 × 1.33	+6.3	45	Yes
Mol 45	18 17 24.50	−17 22 13.0	+47.3	2.90 × 1.38	+4.8	40	Yes
Mol 50	18 19 07.50	−16 11 21.0	+61.8	2.83 × 1.39	+5.2	40	Yes
GGD 27[a]	18 19 12.49	−20 47 23.6	+13.5	3.37 × 1.40	−16.1	65	Yes
Mol 59	18 30 35.20	−10 07 12.0	+93.7	2.54 × 1.43	+2.7	35	No
G31.41+0.31	18 47 34.40	−01 12 45.0	+98.0	2.29 × 1.50	+3.1	40	Yes
Mol 75	18 53 38.10	+01 50 27.0	+57.0	2.20 × 1.51	+6.2	45	Yes
Mol 77	18 55 16.50	+03 05 07.0	+76.0	2.10 × 1.42	+0.1	40	Yes
Mol 82	18 59 03.40	+03 53 22.0	+91.6	2.11 × 1.41	−1.9	40	Yes
Mol 98	19 11 37.40	+08 46 30.0	+57.0	2.02 × 1.47	+5.7	40	Yes
Mol 117	20 11 46.40	+36 49 37.0	−36.4	1.93 × 1.35	−26.9	30	No
Mol 136	21 32 31.50	+51 02 22.0	−46.7	1.90 × 1.19	−22.3	35	Yes
Mol 138[a]	21 40 42.40	+58 16 10.0	− 0.5	2.55 × 1.85	−11.6	40	Yes
Mol 155	23 16 11.70	+61 37 45.0	−51.0	2.05 × 1.25	−6.9	30	No
Mol 160	23 40 53.20	+61 10 21.0	−51.0	2.01 × 1.25	−2.2	30	Yes

NOTE.—Units of right ascension are hours, minutes, and seconds, and units of declination are degrees, arcminutes, and arcseconds.
[a] This source was observed on 2001 November 30 with 20 antennas in the D configuration.

TABLE 5

44 GHz Masers

Source (1)	Maser Number (2)	Maser Peak Position α(J2000) (3)	Maser Peak Position δ(J2000) (4)	S_{max} (Jy) (5)	v_{LSR} (km s^{-1}) (6)	Δv[a] (km s^{-1}) (7)	$\int Sdv$ (Jy km s^{-1}) (8)	Note (9)
S235	1	05 40 53.25	+35 41 46.9	66.50	−16.6	1.5	45.6	
	2	05 40 53.38	+35 41 49.0	0.79	−21.0	0.5	0.29	
	3	05 40 53.40	+35 41 51.0	0.46	−17.1	−17.4 to −16.2	0.51	1
	4	05 40 53.48	+35 41 41.9	1.32	−17.1	0.3	0.41	
	5	05 40 53.60	+35 41 48.9	12.85	−16.2	0.3	3.41	
	6	05 40 53.61	+35 41 49.6	3.09	−15.9	0.3	0.82	
S255	1[b]	06 12 53.63	+18 00 25.1	150.77	11.2	1.7	105.51	2
	2	06 12 53.67	+18 00 27.4	1.21	9.5	1.0	0.92	
	3	06 12 53.75	+18 00 26.8	63.42	10.2	+9.4 to +11.4	47.36	1
	4	06 12 53.76	+18 00 28.4	1.16	8.9	0.50	0.57	
	5	06 12 53.88	+18 00 31.5	1.93	9.5	+7.9 to +9.7	1.72	1
	6	06 12 53.90	+18 00 32.0	1.46	7.2	0.3	0.38	
	7	06 12 53.98	+18 00 14.4	1.23	7.2	0.5	0.47	
NGC 6334F		...	...	>2	−5.0	−2.5 to −9.0	...	3
G5.89−0.39	1[b]	18 00 29.52	−24 03 52.6	15.48	12.2	+11.0 to +12.8	12.55	
	2	18 00 30.36	−24 03 51.6	2.88	12.5	1.0	2.21	
	3	18 00 31.25	−24 03 51.9	9.04	8.7	1.2	4.81	
	4	18 00 31.53	−24 03 50.4	5.75	8.7	0.8	3.27	
	5	18 00 31.62	−24 03 59.5	5.15	8.3	1.0	2.29	
	6	18 00 31.86	−24 03 48.2	9.99	9.2	1.3	5.17	
G8.67−0.36	1	...	...	>4	35.4	3.3	...	3
	2	...	...	>1	33.5	1.3	...	3
G9.62+0.19	1	18 06 15.02	−20 31 40.2	0.93	5.7	+4.7 to +5.8	0.91	
	2[b]	18 06 15.08	−20 31 32.6	2.14	3.7	0.7	1.11	1
	3[b]	18 06 15.29	−20 31 38.6	1.83	3.5	1.0	1.65	1
G10.47+0.03	1[b]	18 08 37.42	−19 51 39.6	1.93	66.7	1.2	1.72	
	2	18 08 37.57	−19 51 40.1	0.32	65.5	0.2	0.11	
	3	18 08 37.79	−19 51 10.6	0.54	62.2	0.3	0.19	
	4	18 08 37.81	−19 51 52.8	0.61	66.7	0.7	0.34	
	5	18 08 37.85	−19 51 13.4	1.27	68.0	+65.3 to +68.3	0.78	
	6	18 08 37.98	−19 51 57.3	0.39	67.7	+66.3 to +68.0	0.29	
	7	18 08 38.13	−19 51 20.8	0.65	64.3	1.3	0.57	
	8	18 08 38.80	−19 51 38.8	1.13	67.7	1.2	0.71	
G10.6−0.4	1	18 10 27.94	−19 55 45.3	3.38	1.6	0.7	1.51	
	2	18 10 29.00	−19 55 48.4	2.90	−7.3	1.2	1.88	
	3	18 10 29.01	−19 55 44.9	5.28	−7.5	1.2	3.42	
	4	18 10 29.03	−19 55 46.2	6.48	−6.8	1.5	4.20	
	5	18 10 29.07	−19 55 48.2	11.76	−6.2	−8.5 to −5.0	21.10	2
	6	18 10 29.08	−19 55 44.8	1.99	−6.0	0.3	0.58	
	7	18 10 29.10	−19 55 47.7	3.66	−6.7	...	...	2
	8	18 10 29.15	−19 55 43.5	4.96	−8.2	1.2	3.45	
	9	18 10 29.33	−19 55 48.2	9.05	−8.8	1.5	5.36	
G12.89+0.49	1	18 11 50.63	−17 31 36.5	15.24	31.5	0.8	7.76	
	2	18 11 50.72	−17 31 37.3	0.83	32.8	0.7	0.42	
	3	18 11 50.74	−17 31 34.9	1.15	34.0	1.0	1.05	
	4	18 11 50.86	−17 31 34.3	0.84	33.7	+33.3 to +35.5	1.32	
	5	18 11 51.03	−17 31 36.5	3.32	32.3	0.8	1.84	
G12.21−0.10	1	18 12 39.86	−18 24 14.5	0.96	27.8	2.3	1.40	
	2	18 12 39.91	−18 24 17.9	1.19	27.2	+25.5 to +29.7	1.75	
	3[b]	18 12 39.96	−18 24 17.5	4.28	23.7	3.3	4.78	
	4	18 12 40.08	−18 24 16.3	3.53	21.3	0.7	0.99	
	5	18 12 40.15	−18 24 15.9	0.37	19.8	+19.5 to +20.5	0.40	
	6	18 12 40.54	−18 24 46.5	2.50	25.7	+24.7 to +26.0	1.78	
G11.94−0.62	1	18 14 02.24	−18 53 32.0	1.38	38.5	+37.8 to +38.8	1.16	
M17		...	...	>2	19.1	0.5	...	3
Mol 45	1	18 17 22.94	−17 22 13.8	2.91	48.3	2.5	3.70	
	2	18 17 23.10	−17 22 14.6	2.89	49.0	1.2	1.70	
	3	18 17 23.29	−17 22 10.0	0.62	49.6	0.5	0.25	
	4	18 17 23.31	−17 22 13.0	0.97	47.6	+45.3 to +48.1	1.69	4
	5	18 17 23.35	−17 22 11.6	5.41	47.3	+45.8 to +47.8	4.67	
	6	18 17 23.84	−17 22 15.3	0.47	49.6	0.3	0.14	
	7	18 17 24.01	−17 22 12.2	1.96	46.8	+45.2 to +49.0	24.85	2,4

TABLE 5—*Continued*

Source (1)	Maser Number (2)	Maser Peak Position α(J2000) (3)	Maser Peak Position δ(J2000) (4)	S_{max} (Jy) (5)	v_{LSR} (km s^{-1}) (6)	Δv[a] (km s^{-1}) (7)	$\int Sdv$ (Jy km s^{-1}) (8)	Note (9)
	8[b]	18 17 24.08	−17 22 14.1	27.45	48.5	...	...	2
	9	18 17 24.22	−17 22 12.6	1.46	47.5	...	...	2
Mol 50	1[b]	18 19 07.64	−16 11 25.6	7.81	62.3	+61.8 to +64.1	5.15	
GGD 27	1	18 19 12.45	−20 47 24.8	154.02	13.2	+12.0 to +15.8	119.02	1
G19.62−0.23	1[b]	18 27 37.44	−11 56 38.4	13.33	41.0	2.8	15.60	5
	2	18 27 37.91	−11 56 34.6	2.48	46.5	+44.0 to +48.1	2.92	1,5
G29.96−0.02[c]	1	18 46 02.58	−02 39 25.5	0.62	97.0	+96.0 to +97.3	0.60	
	2	18 46 03.12	−02 39 28.4	5.06	96.0	+95.8 to +99.8	6.16	
	3	18 46 03.18	−02 39 23.4	0.75	94.7	0.3	0.28	
	4	18 46 03.70	−02 39 27.6	2.94	98.8	1.7	2.71	
G31.41+0.31	1[b]	18 47 34.20	−01 12 49.7	1.65	94.0	0.7	0.72	
	2	18 47 34.34	−01 12 47.7	0.50	101.7	1.8	0.24	
	3	18 47 34.59	−01 12 49.0	1.70	100.2	1.0	1.04	
G34.26+0.15	1	18 53 15.90	+01 15 15.3	1.69	57.8	+57.5 to +62.3	1.72	
	2[b]	18 53 16.10	+01 15 13.3	2.76	57.5	+56.5 to +59.2	3.08	
	3	18 53 16.93	+01 15 10.8	1.22	60.5	+60.3 to +61.3	0.67	
	4	18 53 16.95	+01 15 12.4	0.82	64.0	0.5	0.35	
	5	18 53 17.97	+01 14 55.7	0.30	59.5	+58.5 to +60.0	0.21	
	6	18 53 18.91	+01 14 56.5	11.19	56.3	1.7	9.90	
	7	18 53 19.20	+01 14 48.3	7.74	58.0	+56.7 to +58.8	7.43	
Mol 75[d]	1	18 53 37.71	01 50 25.4	0.67	56.7	0.3	0.26	
Mol 77[d]	1	18 55 16.78	03 05 06.7	0.57	75.7	0.5	0.24	
Mol 82[d]	1	18 59 03.72	03 53 42.9	1.03	90.3	0.5	0.44	
G45.07+0.13[c]	1	19 13 22.04	+10 50 59.0	1.08	59.3	+57.7 to +60.0	1.89	
G45.47+0.07[c]	1	19 14 25.69	+11 09 37.3	0.54	55.9	0.5	0.27	
	2	19 14 25.80	+11 09 20.7	0.55	64.7	0.5	0.17	
	3	19 14 25.84	+11 09 24.3	0.36	59.7	0.3	0.15	
Mol 98	1[b]	19 11 38.78	08 46 37.9	3.84	58.0	1.5	1.62	
	2	19 11 38.78	08 46 33.1	0.91	57.3	0.8	0.51	
	3	19 11 39.15	08 46 30.9	0.41	56.2	0.7	0.25	
W51 N[c]	1	19 23 37.16	+14 31 07.8	5.19	60.0	1.5	3.45	5
	2	19 23 38.75	+14 30 42.2	1.40	61.5	0.5	0.58	5
	3	19 23 39.29	+14 31 03.6	0.98	55.0	0.7	0.56	5
	4	19 23 40.31	+14 31 22.6	0.60	61.4–65.0	0.3	0.22	5
	5	19 23 40.77	+14 31 09.4	0.77	64.2	+62.5 to +64.3	0.42	5
	6	19 23 41.51	+14 31 02.0	1.24	66.6	0.5	0.61	
	7	19 23 42.69	+14 31 33.3	0.85	62.5–65.2	0.3	0.35	
W51 E1	1	19 23 43.40	+14 30 51.1	1.82	59.5	0.5	0.84	
	2	19 23 43.42	+14 30 35.2	1.45	56.5	1.7	1.02	
	3	19 23 43.46	+14 30 35.0	1.27	51.7	+51.0 to +52.3	1.18	1
	4	19 23 43.48	+14 30 35.3	7.79	48.5	1.7	6.04	
	5	19 23 43.64	+14 30 39.0	1.02	56.7	0.3	0.37	
	6	19 23 43.70	+14 30 31.0	0.98	59.3	0.7	0.65	
	7	19 23 43.71	+14 30 41.5	7.26	56.2	1.0	2.87	
	8	19 23 43.71	+14 30 46.2	0.89	58.0	0.8	0.63	
	9	19 23 43.76	+14 30 15.9	2.00	60.6	1.0	1.11	
	10	19 23 43.82	+14 30 34.1	10.73	53.2	1.5	8.88	
	11	19 23 43.95	+14 30 39.9	1.10	56.5	0.7	0.55	
	12	19 23 43.96	+14 30 31.0	75.26	49.2	+47.7 to +51.2	93.03	1
	13	19 23 43.99	+14 30 40.6	1.85	57.0	+56.7 to +58.2	1.86	1
	14	19 23 44.01	+14 30 32.7	2.81	54.0	1.0	1.73	
	15	19 23 44.09	+14 30 41.7	1.20	57.6	1.5	1.23	
	16	19 23 44.10	+14 30 41.8	1.15	56.2	0.7	0.42	
	17	19 23 44.14	+14 30 22.3	0.87	54.8	0.7	0.42	
	18	19 23 44.30	+14 30 39.6	1.94	54.0	1.2	1.79	
	19	19 23 44.30	+14 30 39.3	10.57	55.7	1.0	4.43	
	20	19 23 44.33	+14 30 40.9	2.46	55.2	0.7	1.37	
ON1	1	20 10 08.11	+31 31 33.1	15.30	12.1	0.8	7.19	
	2	20 10 08.79	+31 31 51.2	0.90	9.2	0.5	0.38	
	3	20 10 08.98	+31 31 42.2	2.79	11.4	0.7	1.27	
	4	20 10 10.35	+31 31 21.5	3.06	11.4	0.7	1.16	
20126+4104[d]	1	20 14 25.19	+41 13 35.8	1.70	−2.3	2.7	1.82	1
	2	20 14 25.21	+41 13 35.2	2.27	−2.3	2.2	1.91	

TABLE 5—*Continued*

Source (1)	Maser Number (2)	Maser Peak Position α(J2000) (3)	Maser Peak Position δ(J2000) (4)	S_{max} (Jy) (5)	v_{LSR} (km s^{-1}) (6)	Δv[a] (km s^{-1}) (7)	$\int Sdv$ (Jy km s^{-1}) (8)	Note (9)
	3	20 14 25.33	+41 13 40.1	1.45	−3.2	0.3	0.46	
	4	20 14 25.41	+41 13 38.0	3.91	−3.5	1.7	2.62	
	5	20 14 26.71	+41 13 29.9	2.18	−4.5	0.8	1.03	
ON2.....	1	20 21 44.40	+37 26 48.0	1.63	0.5	0.8	1.17	
	2	20 21 44.68	+37 26 41.3	8.67	3.8	1.0	4.13	
	3	20 21 44.74	+37 26 42.2	6.64	3.1	0.8	3.85	
	4	20 21 44.92	+37 26 56.3	1.87	0.5	0.3	0.63	
W75 N.....	1	20 38 34.98	+42 37 41.7	5.30	10.2	0.5	1.71	
	2	20 38 35.71	+42 37 45.3	1.10	9.6	0.5	0.45	
	3	20 38 35.75	+42 37 42.3	1.16	8.7	0.5	0.37	
	4	20 38 35.98	+42 37 49.7	2.78	8.1	0.5	0.80	
	5	20 38 37.19	+42 37 58.3	46.01	8.9	+8.6 to +9.7	15.79	1
	6	20 38 37.38	+42 37 39.9	5.95	6.7	0.5	1.84	
DR 21(OH)	1[b]	20 38 59.28	+42 22 48.7	236.53	0.5	1.5	133.94	
	2	20 38 59.33	+42 22 47.3	8.81	−1.3	1.3	5.26	
	3	20 38 59.55	+42 22 05.1	1.58	−1.0	0.3	0.45	
	4	20 38 59.87	+42 22 45.8	11.74	−0.7	0.8	6.46	
	5	20 38 59.88	+42 22 49.9	0.91	−10.1	0.7	0.52	
	6	20 38 59.93	+42 22 44.7	24.30	0.1	0.7	11.68	
	7	20 39 00.17	+42 22 47.5	8.99	−1.7	1.8	9.16	
	8	20 39 00.25	+42 22 46.0	48.48	−0.2	2.5	30.23	
	9	20 39 00.53	+42 22 47.5	2.23	1.5	+0.8 to +2.5	2.22	
	10	20 39 01.22	+42 22 40.8	0.85	−3.0	1.0	0.68	
	11	20 39 01.49	+42 22 44.7	1.25	−3.3	−3.7 to −2.5	0.96	
	12	20 39 01.51	+42 22 40.6	5.79	−4.8	2.0	5.53	
	13	20 39 01.67	+42 22 43.1	6.78	−6.7	0.7	2.71	
	14	20 39 02.02	+42 22 40.9	4.66	−4.5	−6.3 to −3.3	10.29	1
	15	20 39 02.07	+42 22 44.9	6.93	−3.7	1.3	3.99	1
	16	20 39 02.17	+42 22 40.9	2.15	−5.3	1.5	2.59	
	17	20 39 02.23	+42 22 43.7	11.33	−5.5	2.2	10.35	
DR 21.....	1	20 39 00.12	+42 19 16.9	1.31	−2.0	0.5	0.60	
	2	20 39 01.76	+42 19 21.1	52.87	−3.6	1.3	25.68	
Mol 136.....	1[b]	21 32 30.82	51 02 14.9	1.12	−47.9	−48.0 to −46.9	0.94	
Mol 138.....	1	21 40 40.95	58 16 16.3	11.63	−0.8	1.0	6.21	
	2	21 40 40.97	58 16 06.8	1.28	−0.0	0.5	0.43	
	3	21 40 41.76	58 16 15.4	4.46	6.5	+4.5 to +8.1	6.46	
NGC 7538.....	1	23 13 43.64	+61 27 52.2	2.00	−59.2	0.7	1.00	
	2	23 13 43.69	+61 27 55.6	5.74	−56.6	0.8	2.47	
	3	23 13 43.93	+61 27 30.4	3.57	−57.2	0.5	1.33	
	4	23 13 45.53	+61 27 41.7	11.97	−57.2	1.2	9.30	1
Mol 160.....	1	23 40 54.46	61 10 30.9	0.66	−49.7	0.3	0.23	
	2	23 40 54.55	61 10 31.0	0.45	−51.0	0.8	0.37	
	3[b]	23 40 54.61	61 10 29.0	1.15	−52.0	0.7	0.55	
	4	23 40 54.74	61 10 28.7	0.52	−51.7	−52.3 to −51.3	0.56	

Notes.—Units of right ascension are hours, minutes, and seconds, and units of declination are degrees, arcminutes, and arcseconds. (1) Possible multiple feature; maser position changes between channels. (2) This maser contains multiple components that cannot be resolved with our spatial resolution. The flux density, line width, and integrated line intensity include the emission from all components present at this spot. (3) Absolute maser positions could not be determined for this source. We give a lower limit to the flux of the strongest maser and the velocity information. (4) This maser appears to have nearby, thermal methanol emission. (5) The positional uncertainty of this maser may be as great as 2″. Table 5 is also available in machine-readable form in the electronic edition of the *Astrophysical Journal Supplement*.

[a] A single number indicates the line width for $S_v > 3\ \sigma$ when there is a single, contiguous run of channels. Two numbers indicates the velocity range for which $S_v > 3\ \sigma$ when a single sky position has multiple, nonadjacent channels above the 3 σ level.

[b] This maser component was used for self-calibration.

[c] Source was self-calibrated using the 23 GHz continuum map.

[d] No self-calibration was applied to this source.

0.2 Jy, more than 10 times more sensitive than previous surveys of this methanol line.

3. RESULTS

Methanol maser emission was detected at 44 GHz in 37 sources of our sample; 23 GHz maser emission was detected in two sources. For most of the targets listed in Tables 2 and 3 the 44 GHz line had been detected previously in single-dish surveys, hence the high detection rate is no surprise. The sample of massive protostellar candidates from Molinari's list, however, had not been searched previously for 44 GHz masers. We observed 12 Molinari sources and detected the 44 GHz line in nine of these, for a detection rate of 75%. These high detection rates show that the 44 GHz line is widespread in young

TABLE 6
23 GHz Masers

Source	Maser Number	Maser Peak Position		S_{max}	v_{LSR}	Δv[a]	$\int Sdv$
		α(J2000)	δ(J2000)	(Jy)	(km s^{-1})	(km s^{-1})	(Jy km s^{-1})
(1)	(2)	(3)	(4)	(5)	(6)	(7)	(8)
W3(OH).....	1	02 27 03.88	+61 52 24.1	9.55	−43.2	3.5	7.3
NGC 6334F.....	1	17 20 53.30	−35 46 55.4	10.9	−10.5	1.3	6.2

Note.—Units of right ascension are hours, minutes, and seconds, and units of declination are degrees, arcminutes, and arcseconds.
[a] Zero power width for S_v greater than 3 σ.

massive star formation regions, ranging from the youngest regions, in a pre-UC H II phase, to more evolved regions, currently in the UC H II phase.

The observed properties of all detected masers are presented in Table 5 (44 GHz) and Table 6 (23 GHz). Column (1) of each table gives the source name, while column (2) identifies each maser component by number, in order of increasing right ascension. Columns (3) and (4) give the peak position for each component, found by fitting a two-dimensional Gaussian to the line channel of peak emission. Coordinates are reported in J2000, although the first and second observing runs were made with B1950 coordinates.

Column (5) gives the peak flux density calculated from a small integration box enclosing the maser. Column (6) gives the LSR-velocity of the channel of peak emission, while column (7) provides the velocity range over which emission occurs. If the line appears as a single feature then we report the FWZI (full width at zero intensity) at the 3 σ level; if multiple velocity components at the same sky position are present then we report the upper and lower velocity bounds at the 3 σ level. In many cases there may be multiple maser features that we do not resolve. Evidence for this is seen by a slight shift of the peak position between channels; such behavior is noted in the footnotes of the tables. Column (8) gives the integrated line flux, calculated as $\Sigma S_i \Delta v_i$ summed over channels above the 3 σ level. In Figures 1–24 we present contour maps of the continuum emission for selected sources, with the positions of the methanol masers indicated as crosses.

3.1. *Sample Spectra*

To indicate the quality of the spectra and to illustrate several interesting cases, we show in Figures 25, 26, 27, and 28 a set of four maser spectra. The survey spectra generally fall into several classes. In some cases, e.g., G11.94−0.62 (Fig. 25), there is a single, isolated maser component. Such components can be quite strong, or, in the case of G11.94−0.62, relatively weak. Of the 169 distinct masers that we catalog, about 77% show this simple spectral structure. These lines are quite narrow with typical line widths of 1.5 km s^{-1} (see Table 5). Another spectral category is an "extended" maser component that shows evidence for marginally resolved spatial and spectral structure. An example of this is maser components 8 and 9 of Mol 45, shown in Figure 26. There are almost certainly two (or more) distinct masers present, but our observations are not able to clearly separate them and measure individual line parameters. Another situation encountered is multiple velocity components at the same sky position. An example is maser component 12 in W51 E1, shown in Figure 27. Typical velocity spreads in these cases are about 4 km s^{-1}; the most extreme

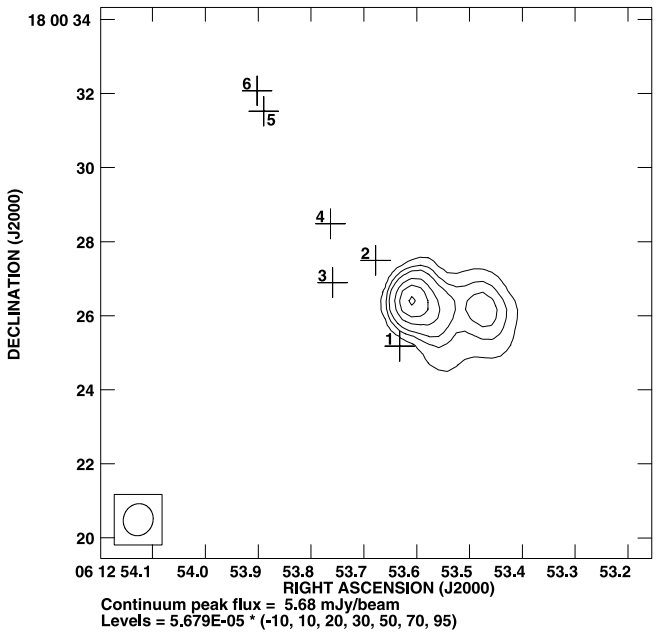

Fig. 1.—S255. The 3.6 cm continuum image is from Kurtz et al. (1994). Numbered crosses indicate 44 GHz methanol masers.

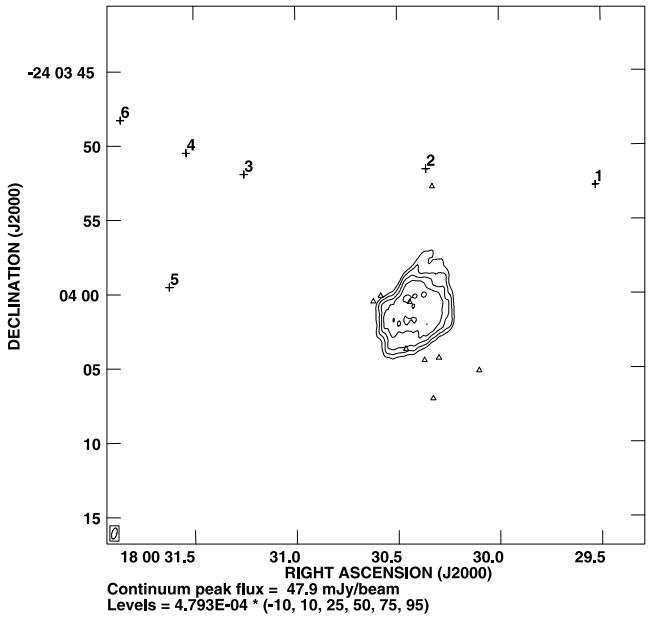

Fig. 2.—G5.89−0.39. The 6 cm continuum image is from WC89. Numbered crosses indicate 44 GHz methanol masers, while triangles indicate water masers reported by HC96. Symbol sizes are generally larger than the positional uncertainty.

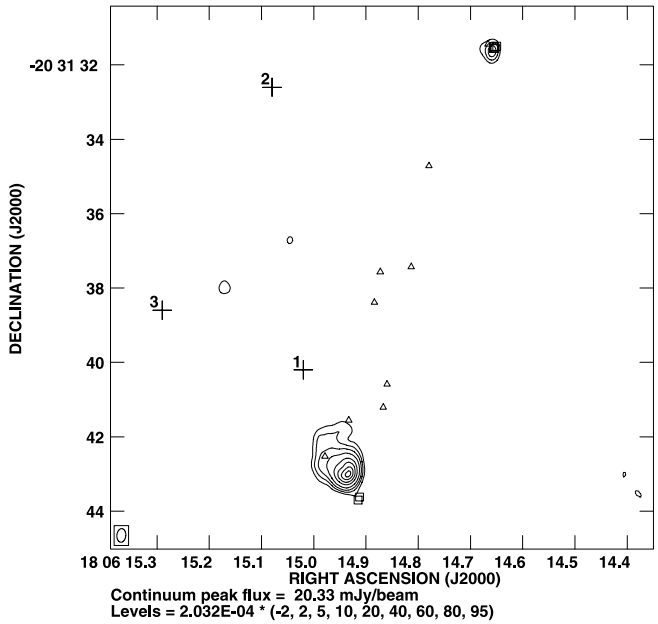

FIG. 3.—G9.62+0.19. The 3.6 cm continuum image is from Testi et al. (2000). The numbered crosses indicate 44 GHz methanol masers while triangles indicate water masers reported by HC96. Squares show the 6.67 GHz methanol masers reported by Walsh et al. (1998).

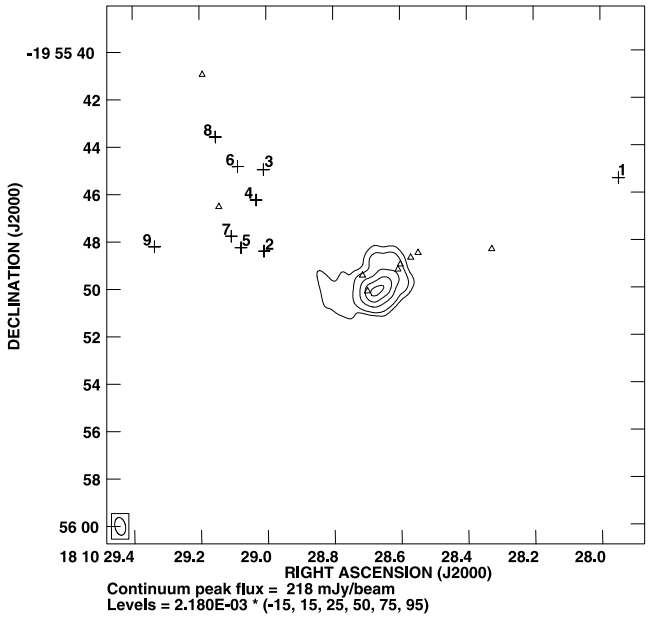

FIG. 5.—G10.62−0.4. Continuum image and maser symbols as in Fig. 2.

case is W51 E1 with a maximum velocity spread of 12.1 km s^{-1}. Finally, two sources (G31.41+0.31 and NGC 7538) showed evidence for thermal methanol emission. The spectrum for the former source is shown in Figure 28.

3.2. *Variability*

About half of our sample has previous observations of the 44 GHz line. A detailed comparison of our results with the published data is often ambiguous because of significant differences in spatial resolution, flux calibration uncertainties, and other factors. Although there is often a substantial difference between published maser fluxes and the values we report here, in general we cannot conclude that the 44 GHz line flux has changed. Two exceptions to this are W3(OH), described in § 3.3.1, and G11.94−0.62. In the case of G11.94−0.62, the VLA and single-dish pointing centers were identical and the maser location is near the center of the primary beam in both cases. Bachiller et al. (1990) report a maser peak flux density of about 45 Jy at about 35 km s^{-1} (see their Fig. 1), where we measured a maser peak flux of 1.38 Jy at about 38 km s^{-1} (see Fig. 25). In this case the difference in measured fluxes is too large to be explained by instrumental

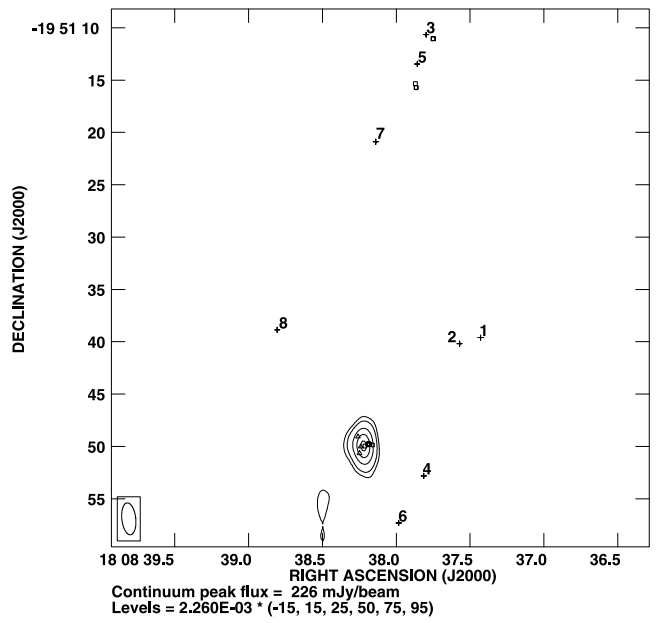

FIG. 4.—G10.47+0.03. 7 mm continuum image from this survey; maser symbols as in Fig. 3.

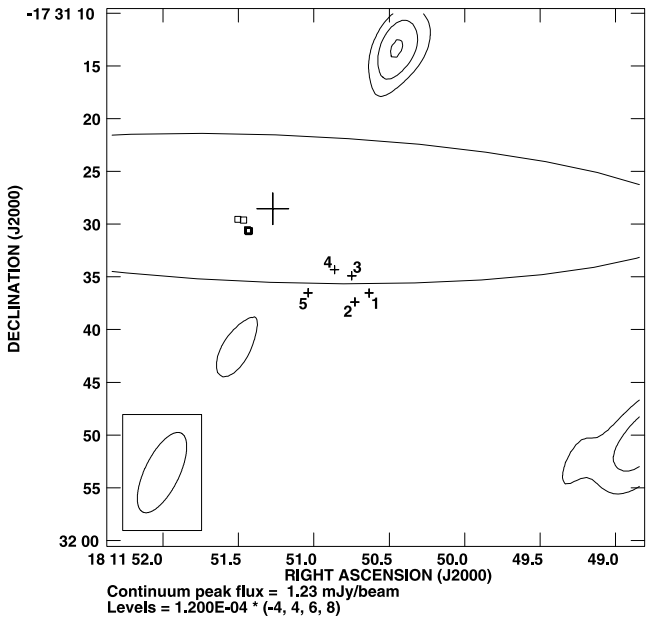

FIG. 6.—G12.89+0.49. Numbered crosses indicate the 44 GHz methanol maser positions; squares show the 6.67 GHz methanol masers reported by Walsh et al. (1998). The 6 cm continuum image was made with VLA archive data from program AH361. Because there is no obvious detection of a compact H II region, we show the position of IRAS 18089−1732, indicated by its uncertainty ellipse with the large cross at the center.

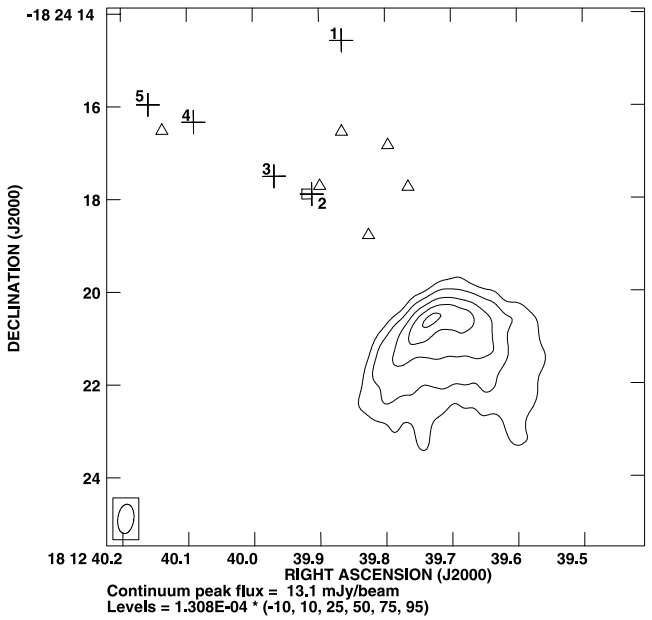

FIG. 7.—G12.21−0.10. Continuum image from WC89 and maser symbols as in Fig. 3. We note the relatively extensive mixing of the different maser species. The 44 GHz maser no. 2 coincides with both a water maser of HC96 and a 6.67 GHz maser of Walsh et al. (1998).

uncertainties, and we conclude that the 44 GHz maser in G11.94−0.62 is variable.

3.3. *Comments on Selected Sources*

3.3.1. *W3(OH)*

No 44 GHz masers were detected in this field, although there is evidence for absorption in the 7_0–6_1 A^+ line. Haschick et al. (1990) report a 44 GHz maser with a peak flux density of about 5 Jy and a velocity of −46.49 km s^{-1}. Our nondetection suggests variability.

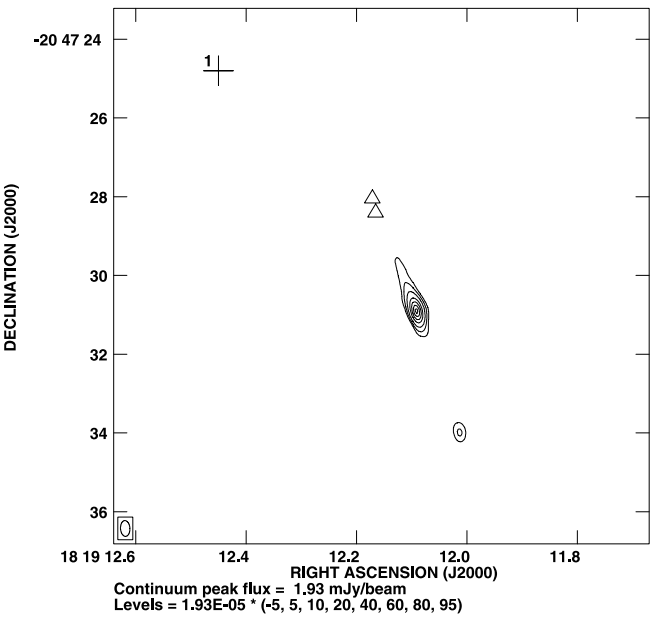

FIG. 8.—GGD 27. The 3.6 cm continuum image is from Gómez et al. (1995). The 44 GHz methanol maser is shown as a cross, while the two triangles show water masers.

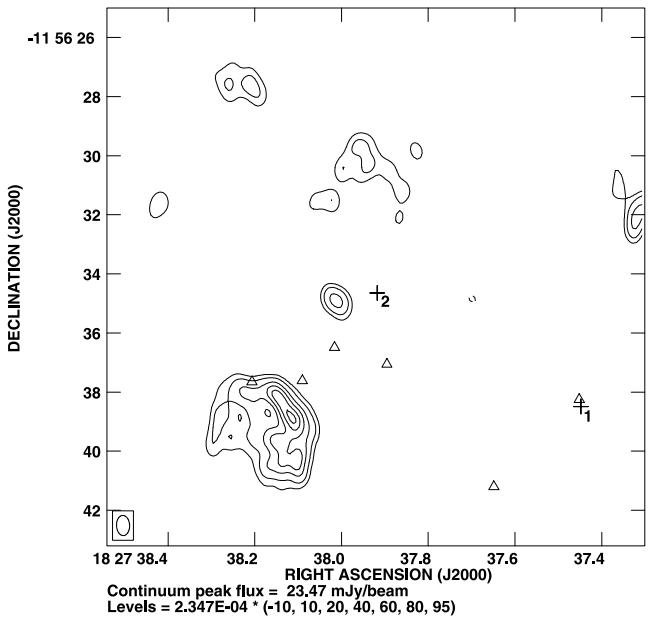

FIG. 9.—G19.62−0.23. Continuum image and maser symbols as in Fig. 2. Methanol maser no. 1 coincides with one of the water masers reported by HC96.

We detect a 23 GHz maser coincident with the UC H II region, covering a velocity range of 3.5 km s^{-1}. At higher spatial and spectral resolution this maser is resolved into multiple components (Menten et al. 1988).

3.3.2. *S235*

This is a prominent region of massive star formation with optical nebulosity (S235A, B, C), H II regions, bright infrared sources (IRS 3, 4), high-density molecular gas and H_2O maser emission (see Felli et al. 1997, 2004 for comprehensive studies). The highly variable H_2O maser (Lo et al. 1975;

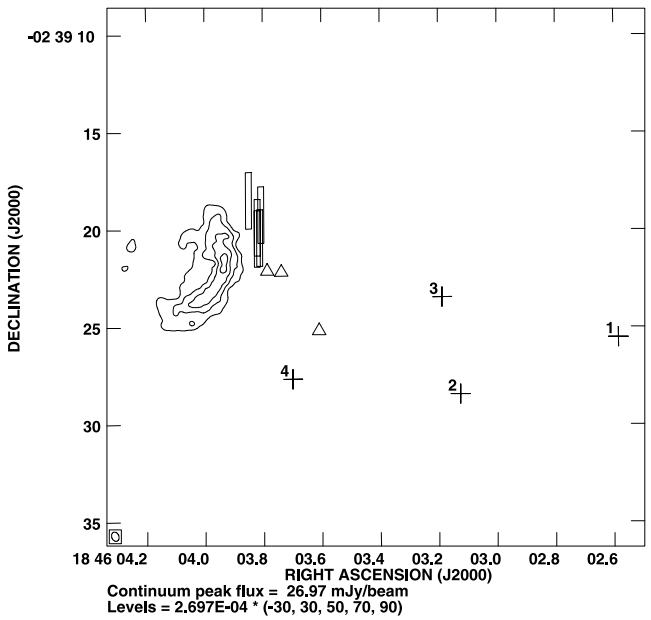

FIG. 10.—G29.96−0.02. Continuum image and maser symbols as in Fig. 3, although here the squares of the 6.67 GHz methanol masers of Walsh et al. (1998) are shown as rectangles, reflecting the larger declination uncertainty for this high-latitude southern source.

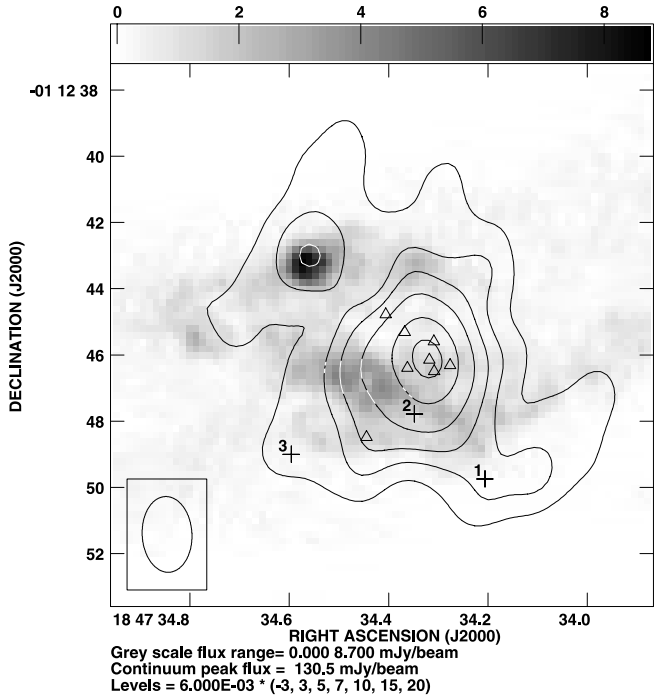

FIG. 11.—G31.41+0.31. The gray-scale shows 6 cm continuum emission; from WC89. The contours show 7 mm nonmaser emission from this survey, a mixture of continuum and thermal methanol (see § 3.3.5). Crosses show the 44 GHz methanol masers while triangles show the HC96 water masers. At centimeter wavelengths the emission is dominated by the UC H II region in the northeast, while the extended nebulosity to the southwest is nearly resolved out. Both the methanol and the water maser emission are associated with the HMC rather than the UC H II region. The methanol masers we detect coincide with the peak of the shock-tracing SiO emission reported by Maxia et al. (2001; see their Fig. 7).

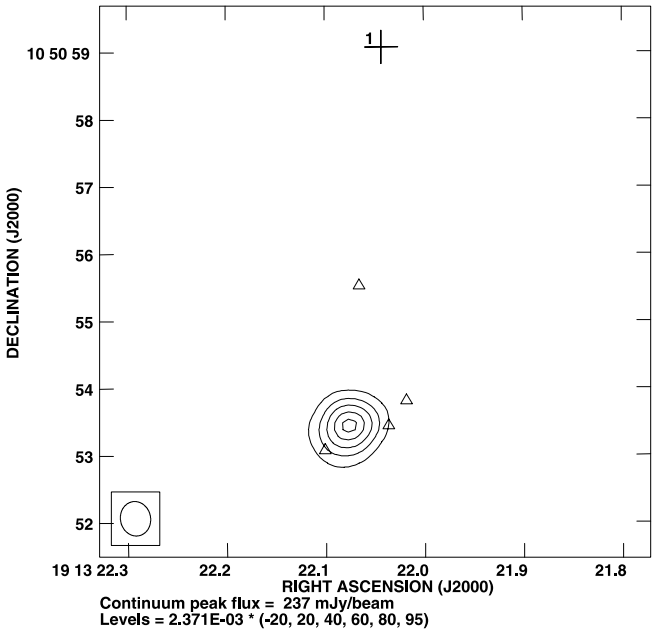

FIG. 13.—G45.07+0.13. Continuum image and maser symbols as in Fig. 2.

Tofani et al. 1995) is located between S235A and B at the peak position of a hot molecular core, coincident with a highly reddened NIR source showing no radio continuum emission, and is thus an excellent candidate for a massive star in a very early stage of evolution.

We detect a cluster of five 44 GHz masers within a distance of about 2″ (0.02 pc) around the position of the H_2O maser, with methanol maser no. 2 coincident with the H_2O maser. While the H_2O maser has shown variable emission over a large velocity range, the velocities of the 44 GHz methanol masers all cluster around 17 km s^{-1}—the velocity of the HMC as traced by ^{34}CS(3–2) (Felli et al. 1997). An attractive explanation of this source is a very young, massive object with

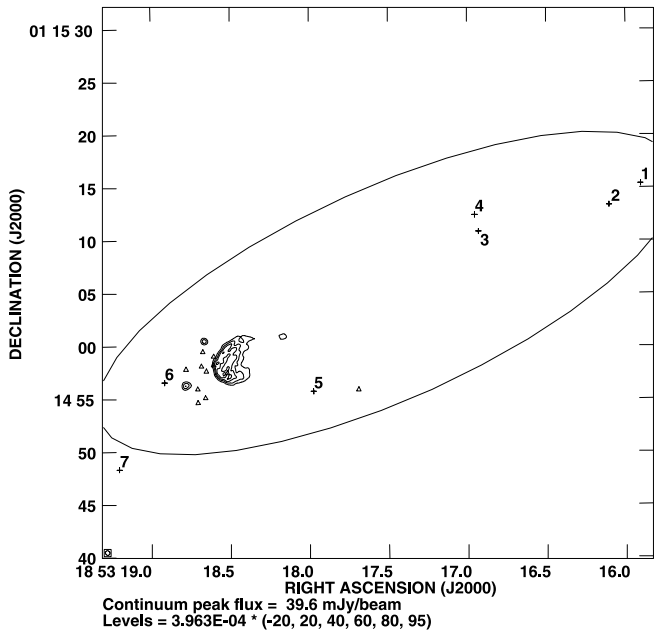

FIG. 12.—G34.26+0.15. The continuum image and maser symbols are as in Fig. 2. The ellipse shows the approximate orientation and spatial extent of the SiO emission reported by Hatchell et al. (2001).

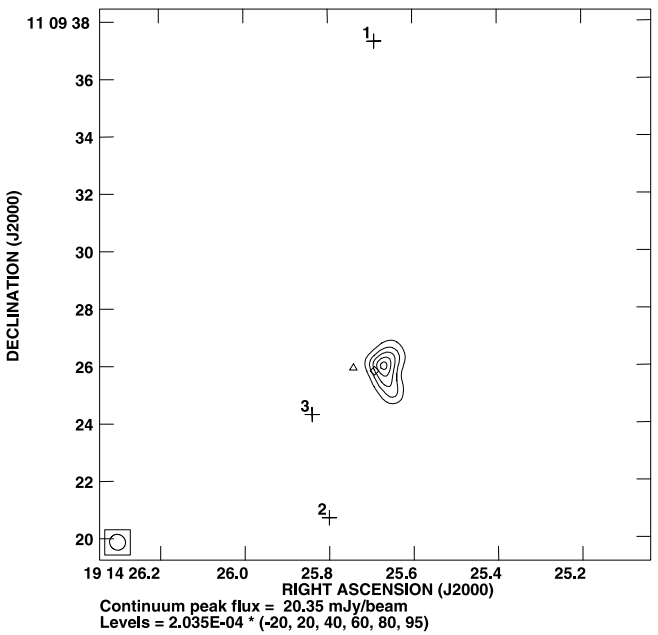

FIG. 14.—G45.47+0.07. The continuum image is from WC89. Crosses show 44 GHz methanol maser positions. The diamond indicates an OH maser and the triangle a water maser; both reported by Forster & Caswell (1989).

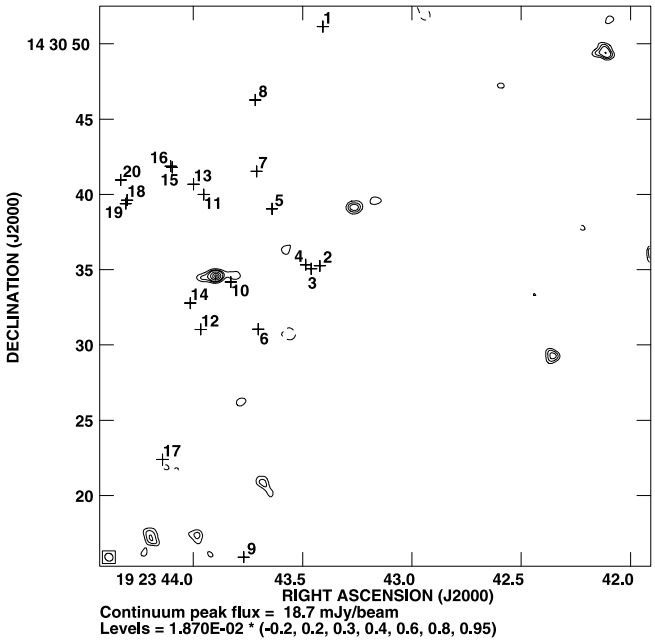

FIG. 15.—W51 E1. Continuum and masers as in Fig. 2. This region of the W51 cloud is quite rich in 44 GHz maser emission, with 20 distinct masers within the 1′ primary beam. This is in contrast to the W51 N region of the molecular cloud (shown in Fig. 16) where only three masers were detected within the primary beam. Moreover, the W51 E1 masers are in relatively close proximity to the H II region E1 (WC89), whereas the W51 N masers are further from the H II region.

variable winds or jets that result in shocked gas in the acceleration region from which the H_2O maser arises, and the methanol masers occur farther out in the flow at the interface with the surrounding molecular core gas.

3.3.3. *G9.62+0.19*

We report three 44 GHz masers for this field. None of these maser positions show continuum emission in the high-sensitivity images of Testi et al. (2000) to 5 σ levels of 0.1 mJy at 3.6 cm and 5 mJy at 7 mm. All three of the masers, however, do coincide with the molecular outflow surrounding the HMC G9.62+0.19-F, mapped in HCO^+ by Hofner et al. (2001).

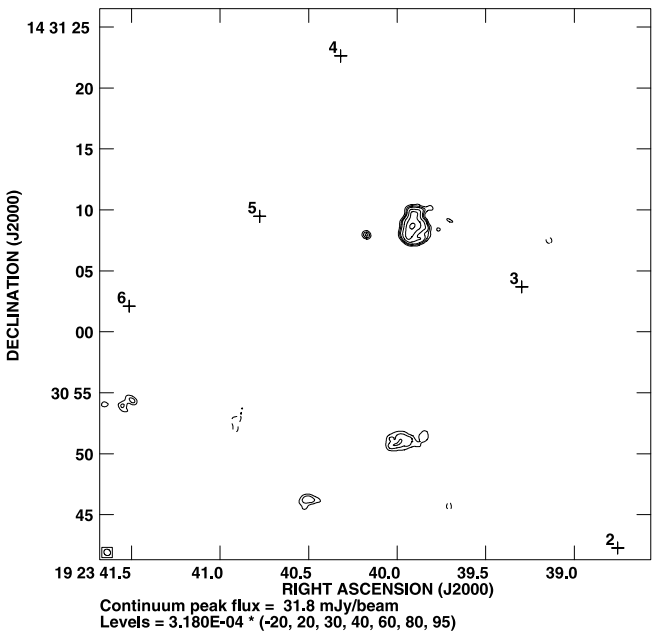

FIG. 16.—W51 N. Continuum and masers as in Fig. 2. This region of the W51 cloud, about 2 pc to the northwest of W51 E1 shown in Fig. 15, is sparsely populated in 44 GHz masers. Only three components lie within the 1′ primary beam; none of them are closer than 0.35 pc to the H II region.

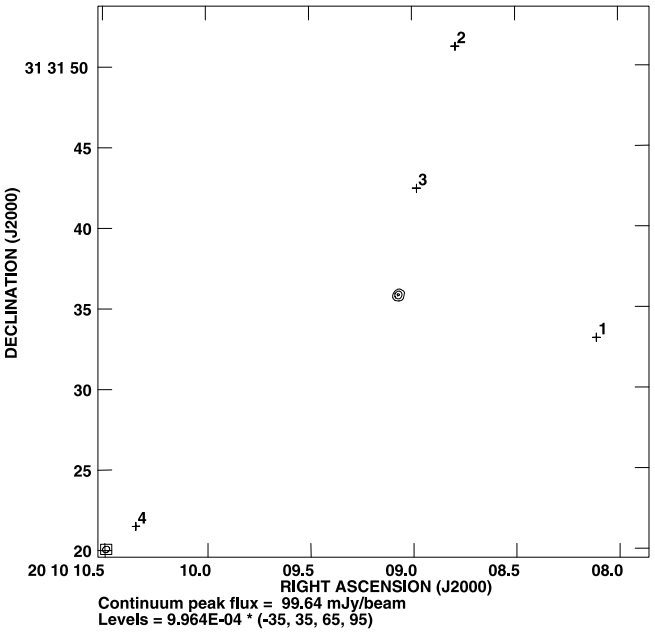

FIG. 17.—ON1. The continuum image is from this survey. The crosses show 44 GHz methanol masers. The methanol masers in this field are relatively well-separated from the radio continuum emission. Zheng et al. (1985) report water and hydroxyl masers coincident with the continuum source.

3.3.4. *G12.21−0.10*

With the exception of one maser (no. 6) all the 44 GHz masers that we detect are clustered 3″–8″ to the northeast of the cometary UC H II region. Hofner & Churchwell (1996, hereafter HC96) detected a cluster of water masers in roughly the same position. The majority of the 6.67 GHz masers reported by Walsh et al. (1998) are more than 30″ from the UC H II

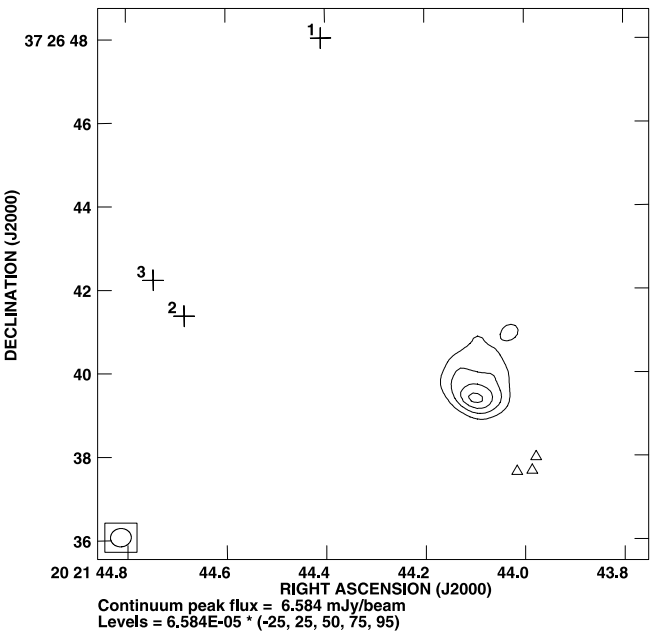

FIG. 18.—ON2. Continuum image and maser symbols as in Fig. 2.

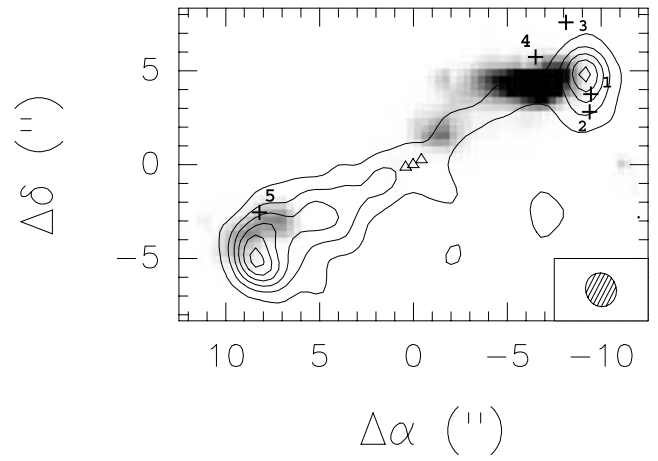

FIG. 19.—IRAS 20126+4104. Contours show SiO (2–1) emission, while gray-scale shows H_2 emission (Cesaroni et al. 1999a, 1997). Triangles indicate water masers (Tofani et al. 1995) while numbered crosses are 44 GHz methanol masers. The reference position is (J2000) R.A. $20^h14^m26^s.03$, decl. $41°13'32''.5$. The methanol masers appear to trace the edge of the shocked gas seen in H_2.

region and the maser cluster. Nonetheless, the strongest maser they find (component E) is coincident with our maser no. 2, although there is a 7.5 km s^{-1} velocity difference between them. Also coincident with this position is water maser no. 1 from HC96, whose velocity is close to that of the 6.67 GHz maser; see Fig. 7. Such a spatial coincidence of class I (44 GHz), class II (6.67 GHz) and water masers is not consistent with the traditional definition of class I and II methanol masers (see § 4.1).

3.3.5. *G31.41+0.31*

Wood & Churchwell (1989, hereafter WC89) reported G31.41+0.31 as core-halo morphology UC H II region and Cesaroni et al. (1994) discovered a HMC about 5″ to the SW of the UC H II "core" position. This object is one of the most

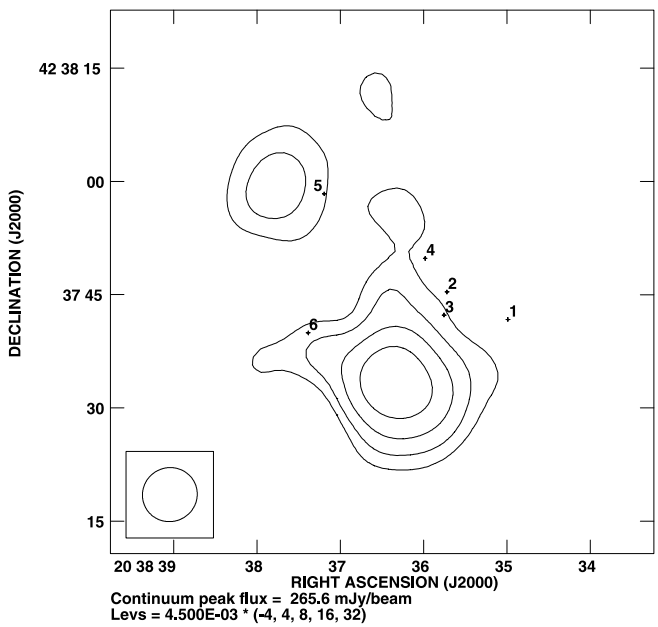

FIG. 20.—W75 N. Contours show 3 mm continuum emission from Shepherd et al. (2003); crosses show 44 GHz methanol maser positions.

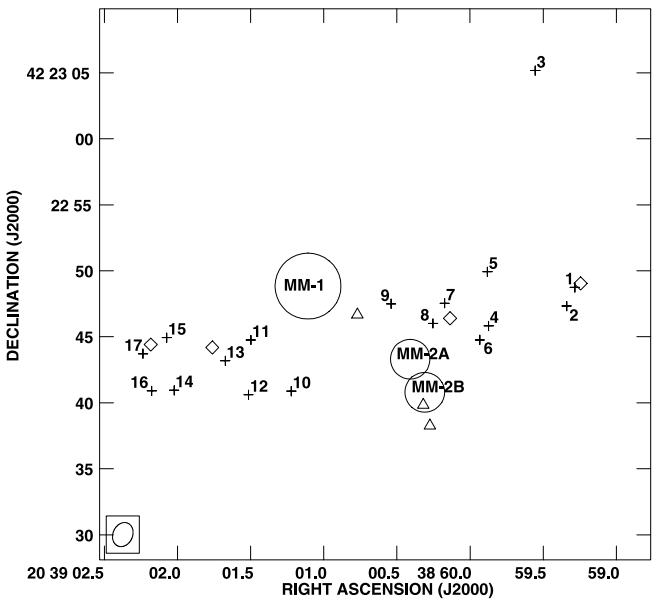

FIG. 21.—DR 21(OH). We did not detect continuum emission in this field. Indicated are the positions of the 44 GHz methanol masers we detect (*crosses*), the ammonia emission (*circles*) and water masers (*triangles*) reported by Mangum et al. (1992), and the 95 GHz methanol masers (*diamonds*) reported by Plambeck & Menten (1990). See discussion in text, § 3.3.8.

prominent HMCs in the galaxy and has been studied in many different molecular lines (e.g., Cesaroni et al. 1999b; Olmi et al. 1996b). In particular, Olmi et al. (1996a) reported outflow activity from the HMC and Maxia et al. (2001) found SiO(2–1) emission of 10″ extent coincident with the HMC. The HMC is also outlined very well with H_2O masers (HC96).

We detect three 44 GHz masers located along the southern edge of the HMC, and coincident with the SiO emission imaged by Maxia et al. (2001). We also detect a very broad thermal methanol emission line that essentially filled our

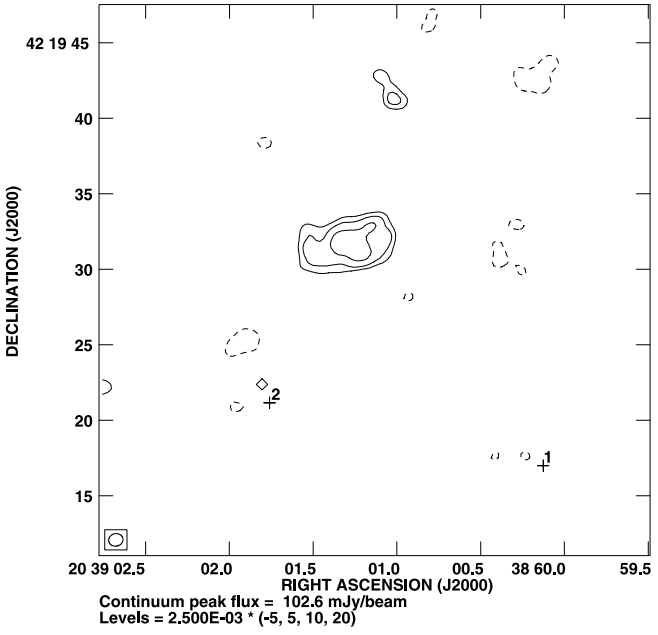

FIG. 22.—DR 21. The 3.6 cm continuum image is from Kurtz et al. (1994). Crosses show 44 GHz methanol maser emission, while the diamond denotes the 95 GHz methanol maser reported by Plambeck & Menten (1990).

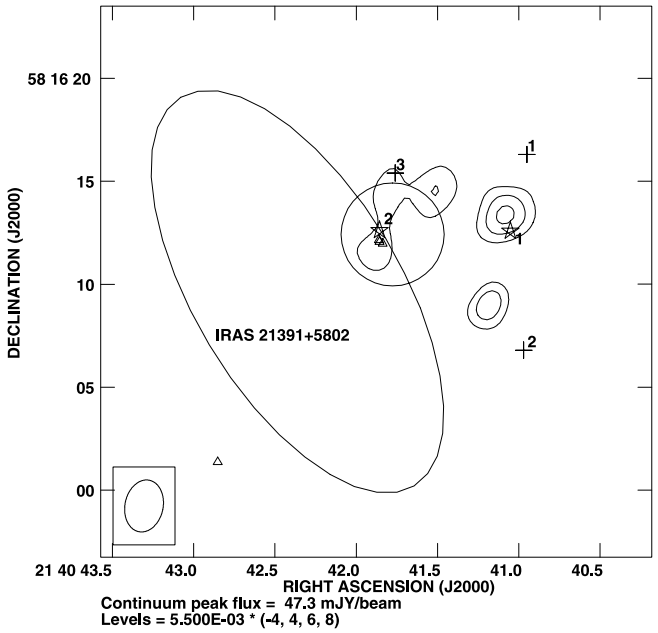

FIG. 23.—Mol 138. The 44 GHz methanol masers are indicated by crosses; IRS 1 and IRS 2 are indicated by numbered stars; water masers (Tofani et al. 1995) are shown by triangles. The 2.7 mm continuum is shown by a 5″ diameter circle; this is the upper limit to the source size determined by Wilking et al. (1993). Because there is no compact H II region present in this field, we also show the *IRAS* positional uncertainty ellipse for 21391+5802. Contours show the 7 mm continuum emission that we detect in the line-free channels; contours are −4, 4, 6, and 8 times the image rms of 5.5 mJy beam^{-1}.

bandpass (see Fig. 28). By mapping the maser-free channels it is possible to estimate the location of the thermal methanol emission, although there may be some contamination from continuum emission that we are unable to subtract owing to the lack of line-free channels. Despite this uncertainty, we find that, similar to many other high-density molecular tracers, the CH_3OH thermal emission peaks at the position of the HMC.

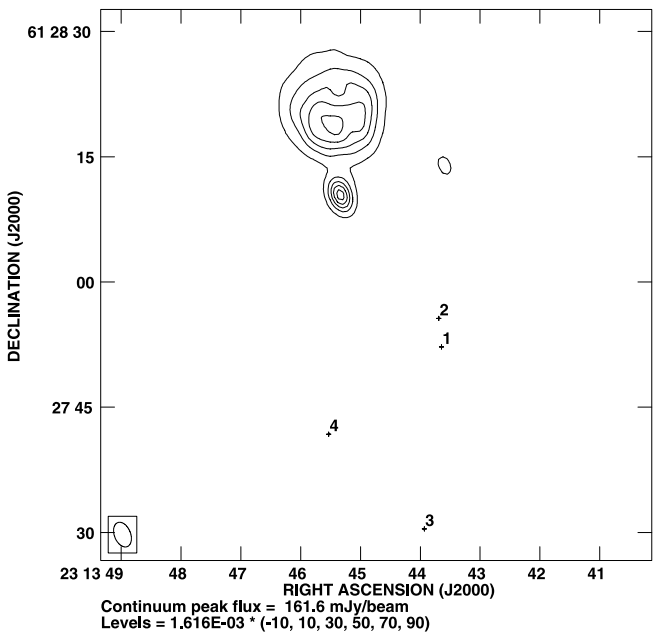

FIG. 24.—NGC 7538. The 3.6 cm continuum image is from Sewilo et al. (2004); 44 GHz masers are shown by crosses.

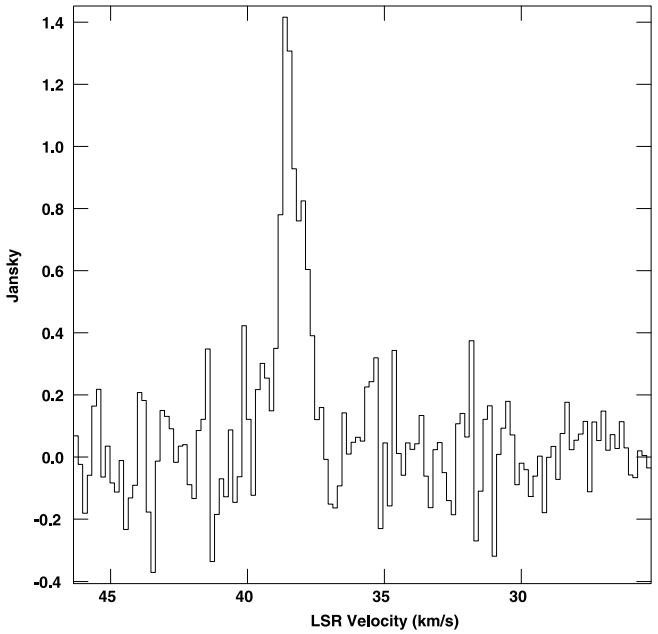

FIG. 25.—44 GHz spectrum of the isolated, variable maser near G11.94−0.62.

A Gaussian fit to the thermal line profile yields a line center velocity of 98.6 ± 0.1 km s^{-1} and a FWHM of 7.9 ± 0.3 km s^{-1}. Higher spatial resolution observations (E. Araya et al. 2004, in preparation) suggest that the thermal methanol emission traces an outflow centered on a central young stellar object.

3.3.6. *G34.26+0.15*

G34.26+0.15 is a well-studied massive star formation region harboring an extended H II region, a cometary UC H II region and two hypercompact H II regions along with a HMC (e.g., WC89; Fey et al. 1992; Gaume et al. 1994; Heaton et al. 1993; Garay & Rodríguez 1990) and several infrared and molecular

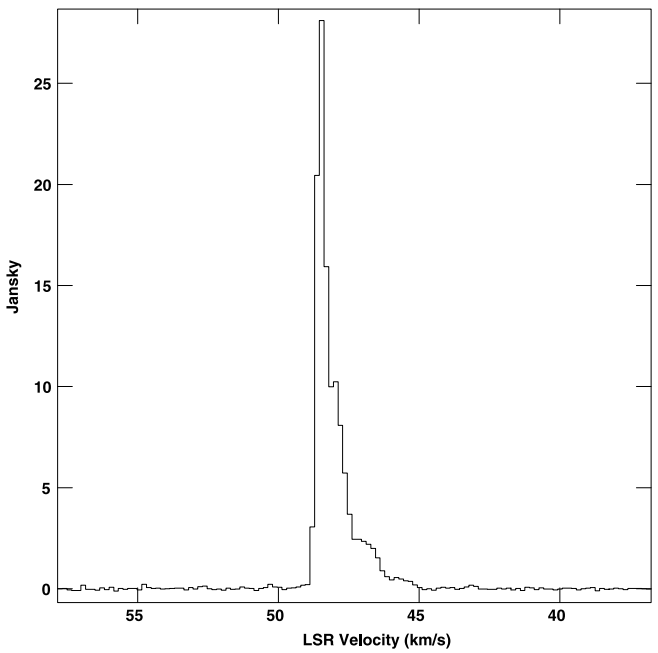

FIG. 26.—44 GHz spectrum of marginally resolved maser spots 8 and 9 in Mol 45, integrated over the area of maser emission.

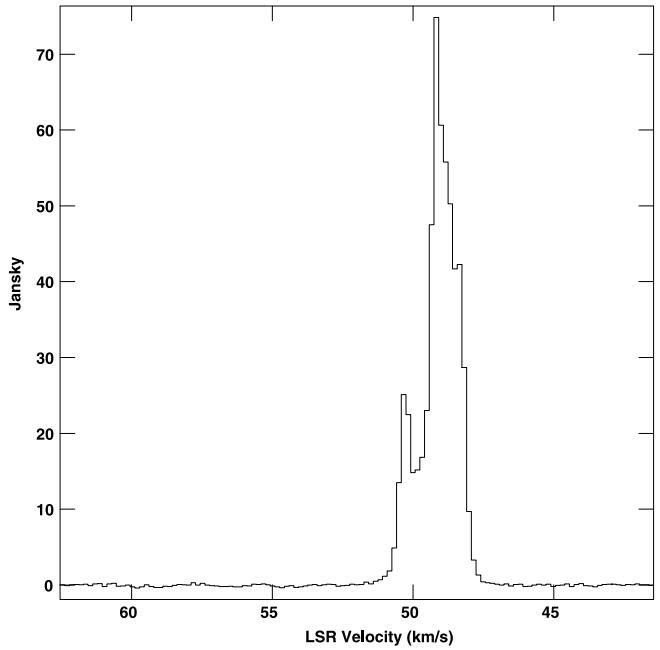

FIG. 27.—44 GHz spectrum of multiple velocity components from the same sky position, maser no. 12, in W51 E1.

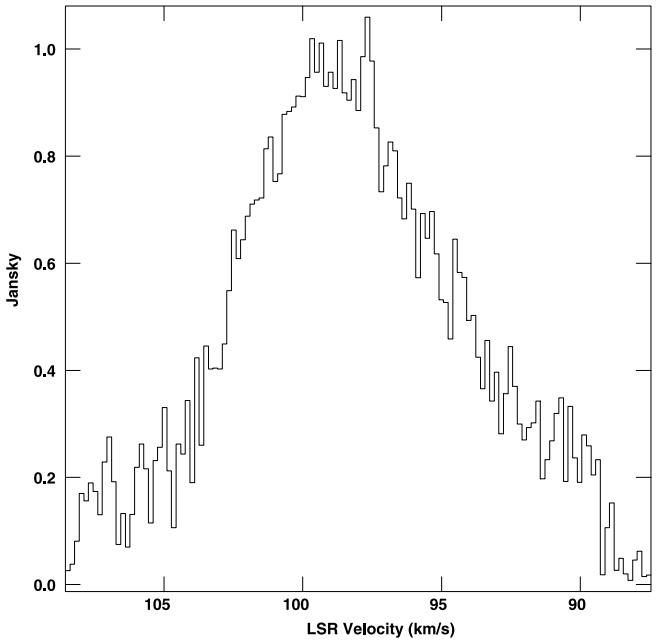

FIG. 28.—44 GHz spectrum of G31.41+0.31, showing thermal methanol emission which nearly fills the bandpass. Continuum emission has *not* been subtracted from this spectrum. The continuum level appears to be about 0.2 Jy, but there are insufficient line-free channels to perform a reliable subtraction.

line sources (e.g., Campbell et al. 2000). We detect seven distinct 44 GHz masers, which are located in an area about $1' \times 20''$ oriented approximately in the SE-NW direction. A comparison with the SiO(1–0) map of Hatchell et al. (2001) shows that the 44 GHz maser distribution, extent, and velocities are nearly identical to those of SiO [although the masers appear to avoid the SiO(1–0) peak positions]. This provides strong evidence that the 44 GHz masers arise from shocked gas in molecular flows.

3.3.7. *IRAS 20126+4104*

This source is a well-known, very young massive object prior to the UC H II region phase of development (Cesaroni et al. 1997, 1999a; Hofner et al. 1999). A luminous ($L_{\rm bol} \approx 10^4\ L_\odot$) central source is embedded in a HMC and drives a massive bipolar flow in the SE-NW direction, nearly in the plane of the sky. This flow has been mapped in CO isotopes over distances of several arcminutes (Shepherd et al. 2000), and in the HCO^+ molecule over tens of arcseconds (Cesaroni et al. 1997). In the inner $10''$ the presence of shocked gas is evident from an SiO jet and strong emission in the H_2 $v = 1 \rightarrow 0$ $S(1)$ vibrational line at 2.122 μm (Cesaroni et al. 1997).

We detect five 44 GHz masers toward IRAS 20126+4104, that are located about $8''$ to the SE and NW of the central object, i.e., along the axis of the bipolar molecular flow. As seen in Figure 19, maser components 1–4 are located along the edge of the NW SiO jet, while maser 5 is located on the edge of the SE SiO jet. These locations strongly suggest that the masers originate in the interface between the hot, shocked molecular gas and the surrounding core.

3.3.8. *DR 21(OH)*

DR 21(OH) is particularly rich in the 44 GHz maser line. We detect emission from 17 distinct locations with the strongest emission line strength of 133 Jy. Most of the masers occur in two clusters that are located almost symmetrically to the east and west of DR 21(OH)-MM1, with a total angular spread of about $30''$ (see Fig. 21). Similar structure is seen in the high angular resolution observations ($0''.2$) of the 44 GHz line by Kogan & Slysh (1998) and in the low angular resolution ($5''$) 95 GHz $8_0 \rightarrow 7_1$ A^+ observations by Plambeck & Menten (1990). There is a clear velocity difference of about 5 km s^{-1} between the two clusters with the eastern group having more negative velocities. The velocity of DR 21(OH)-MM1 as measured from NH_3(1, 1) (Mangum et al. 1992) is almost exactly between the mean velocities of the two maser lobes, but neither it, nor the other ammonia cores detected by Mangum et al. are perfectly centered between the two lobes of methanol masers. Nevertheless, millimeter continuum, ammonia line, and water maser emission are clearly confined to an area that separates the two lobes. Thus, an attractive explanation of the data is a scenario in which the methanol masers in DR 21(OH) originate in a bipolar outflow. The driving source of the putative flow is still unknown.

3.3.9. *Mol 136 and Mol 160*

Mol 136 and Mol 160 are the only two Molinari sources common to this survey and the molecular line study of Molinari et al. (2002). For both sources, the 44 GHz masers that we detect coincide with the peak of the HCO^+ and the 3.4 mm continuum emission reported by Molinari et al. (see their Fig. 1).

3.3.10. *Mol 138*

This source is better known as IC 1396 North. We detect three maser components in the field. In Figure 23 we show the position of these three, along with the positions of water masers (from Tofani et al. 1995), infrared sources and millimeter-continuum (from Wilking et al. 1993) and the IRAS 21391+5802 position ellipse. Also shown is weak 7 mm continuum emission that we detect in the line-free channels. None of the methanol masers coincide with other features, but rather fall $3''$ to $5''$ distant from them (0.01 to 0.02 pc for an adopted 750 pc distance based on its association with Cep OB2).

TABLE 7
44 GHz Maser Offset Information

Source	Reference Position[a]		Distance (kpc)	Distance Reference
	α (J2000)	δ (J2000)		
S235	05 40 52.84	+35 42 18.8	1.8	1
S255	06 12 53.55	+18 00 26.1	2.4	2
G5.89−0.39	18 00 30.42	−24 04 01.5	2.0	3
G9.62+0.19	18 06 14.95	−20 31 43.0	5.7	4
G10.47+0.03	18 08 38.24	−19 51 50.0	5.8	5
G10.6−0.4	18 10 28.70	−19 55 50.0	6.0	6
G12.21−0.10	18 12 39.70	−18 24 21.0	13.5	7
G11.94−0.62	18 14 01.13	−18 53 25.2	4.3	8
G19.62−0.23	18 27 38.15	−11 56 39.0	3.5	5
G29.96−0.02	18 46 04.00	−02 39 22.0	6.0	9
G31.41+0.31	18 47 34.56	−01 12 43.3	7.9	5
G34.26+0.15	18 53 18.50	+01 14 58.0	3.7	10
G45.07+0.13	19 13 22.08	+10 50 53.5	6.0	10
G45.47+0.07	19 14 25.67	+11 09 26.0	6.0	10
W51 N	19 23 39.91	+14 31 08.7	7.0	11
W51 E1	19 23 43.89	+14 30 34.3	7.0	11
ON1	20 10 09.97	+31 31 35.9	3.0	10
20126+4104	20 12 26.02	+41 13 32.7	1.7	12
ON2	20 21 44.10	+37 26 39.5	5.0	13
W75 N	20 38 36.40	+42 37 35.0	2.0	14
DR 21	20 39 01.33	+42 19 31.6	2.0	15
NGC 7538	23 13 45.40	+61 28 15.0	2.8	16

[a] J2000 position corresponding to geometric center of centimeter continuum emission. Units of right ascension are hours, minutes, and seconds, and units of declination are degrees, arcminutes, and arcseconds.

References.—(1) Evans & Blair 1981; (2) Hunter & Massey 1990; (3) Acord et al. 1998; (4) Hofner et al. 2001; (5) Churchwell et al. 1990; (6) Downes et al. 1980; (7) S. Kurtz et al. 2004, in preparation; (8) Sewilo et al. 2004; (9) Pratap et al. 1999; (10) Araya et al. 2002; (11) Genzel et al. 1981; (12) Cesaroni et al. 1997; (13) We adopt 5.0 kpc, intermediate between 4.3 kpc (Bronfman et al. 1996) and 5.5 kpc (Reifenstein et al. 1970); (14) Association with Cygnus; (15) Roelfsema et al. 1989; (16) Campbell & Thompson 1984.

3.3.11. *NGC 7538*

The NGC 7538 field contains both ultra and hypercompact H II regions (Gaume et al. 1995). The hypercompact region (IRS 1) shows emission in both the 6.67 GHz and the 12.2 GHz maser lines and has been well-modeled as an edge-on disk (Pestalozzi et al. 2004). We detect four 44 GHz masers, all offset from IRS 1 by more than 15″.

We also detect emission in the 9_2–10_1 A^+ transition at 23 GHz, centered at the position of IRS 1. The spectrum shows several relatively weak and narrow features superimposed on an even weaker plateau of emission. A two-component Gaussian fit to the strongest, central peak and to the emission plateau yields a line center velocity of -56.2 ± 0.2 km s^{-1} and a FWHM of 1.1 ± 0.5 km s^{-1} for the central peak. Corresponding values for the plateau are -56.5 ± 0.5 and 7.7 ± 1.5 km s^{-1}.

4. DISCUSSION

4.1. *Occurrence of Methanol Masers with Respect to Other Sources*

The methanol maser classification scheme was introduced by Batrla et al. (1987) and was further refined by Menten & Batrla (1989), Haschick et al. (1989), Plambeck & Menten (1990), and Menten (1991). The classification was based on several factors, including the association with other astronomical sources, which transitions were present or absent (or seen in emission or absorption), and the complexity of the spectral features and their similarity (or lack thereof) to spectra of other maser species.

Of particular relevance here is that class I masers were typically found to be offset by one or two parsecs from other star formation signposts such as H II regions and water masers, while class II masers were found in close association with these signposts. Although this was a reasonable criterion at the time, based on the mostly low spatial resolution data that were then available, more recent data suggest a revision of this criterion. Slysh et al. (1994) note that there can be considerable overlap between class I and II masers within a single field, especially when neither species has particularly strong emission. They favor a definition of class I/II masers based strictly on the emitting transitions, rather than association with other astronomical objects.

Our data appear to support the position of Slysh et al. (1994). In our sample there are 22 fields with compact H II regions at known distances that show 44 GHz maser emission. For these 22 fields we have calculated the projected linear distance from each maser component to the geometric center of the H II region. The sources included in this calculation are indicated in Table 7. A histogram of the resulting distances (Fig. 29) shows that although some maser-to-H II region offsets as large as 1–2 pc do occur (in particular, six, or 5% of the 118 distances graphed), they are the exception rather than the rule. The vast majority of the separations (102 or 86%) are less than 0.5 pc, with 0.2 pc being the median separation.

Visual inspection of Figures 1–24 shows that water masers usually are closer to the H II region than are the 44 GHz methanol masers. Indeed, HC96 reported a median separation of 0.1 pc between water masers and the continuum peak.

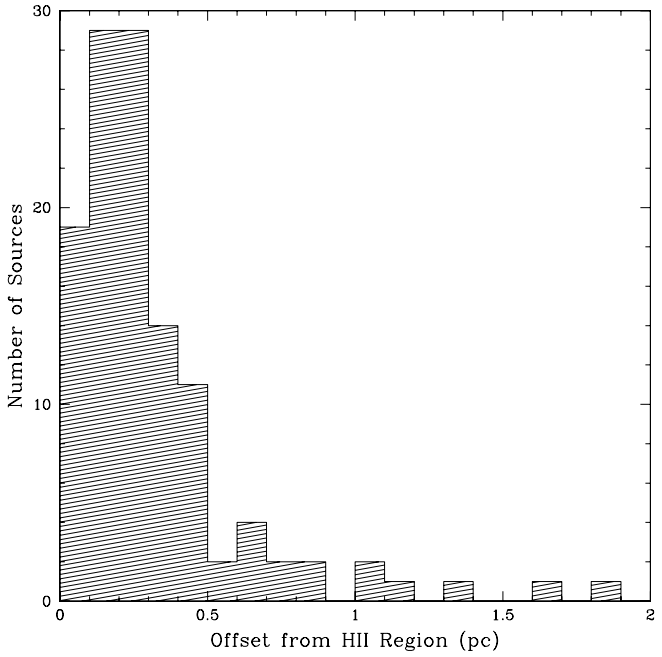

FIG. 29.—Histogram of the linear projected offset between compact H II regions and 44 GHz masers. Sources represented in the histogram and their adopted distances are given in Table 7. Most masers are closer to ionized regions than the 1 pc distance suggested by the original class I definition. See the discussion in § 4.1.

In addition, different maser species (H_2O, 6.67 GHz and 44 GHz methanol) are often uncorrelated—and occasionally anticorrelated—with one another. Nevertheless, we do find some cases (e.g., G12.21−0.10 and G19.62−0.23) in which 44 GHz masers spatially coincide (within our resolution) with water or 6.67 GHz (class II) methanol masers. This suggests that the mutual exclusivity between class I methanol masers and water or class II methanol masers may not be as strong as suggested by the original classification scheme.

The 23 GHz 9_2–10_1 A^+ transition is a class II methanol maser and hence is expected to be found in close association with H II regions and other massive star formation phenomena. Of the 31 fields we observed in this line, 28 have H II regions, yet only two showed 23 GHz maser emission. How are we to understand this extremely low detection rate?

A possible explanation comes from Walsh et al. (2003), who note that their previous work has shown that 6.67 GHz class II masers are often *not* associated with UC H II regions. They suggest two interpretations: that 6.67 GHz masers occur at an earlier stage, before H II regions form, or that this class II maser is pumped by lower mass stars that are unable to form an H II region. In the former case they suggest that the formation of the H II region acts to terminate the conditions for this class II maser emission. If this is the case, it could explain the extreme absence of 23 GHz masers in our sample, in which most fields have already developed UC H II regions.

Nevertheless, of the 28 fields with compact H II regions that we observed in the 23 GHz line, 12 were observed in the 6.67 GHz class II line by Walsh et al. (1998) with a 100% detection rate. We detect 44 GHz masers in 24 of the 28, and 23 GHz masers in only 2 of the 28. Thus, in our sample, the presence of compact H II regions correlates quite well with *both* class I (44 GHz) *and* class II (6.67 GHz) masers. The 23 GHz class II maser, however, is notably rare. The paucity of 23 GHz masers was noted by Cragg et al. (2004), who observed 50 southern sources and report a single 23 GHz maser detection. We refer the reader to their paper, which includes a discussion of the physical conditions of the interstellar gas and dust that affect the pumping of this maser transition. We interpret the rarity of the 23 GHz (class II) maser, coupled with the high detection rate of both 6.67 GHz (class II) and 44 GHz (class I) masers in fields with compact H II regions, to support the view of Slysh et al. (1994) that methanol masers should be classified by transition, not by association with other astronomical objects.

4.2. *The Relation of Methanol Masers with Molecular Outflows*

Based on their interferometric images of the 95 GHz 8_0–7_1 A^+ methanol masers in DR 21, Plambeck & Menten (1990) proposed that class I methanol masers might be associated with molecular outflows. Johnston et al. (1992) concur, based on the 25 GHz class I methanol masers in Orion. In both cases the distribution of class I masers correlates with H_2 emission, indicating a relation to shocked molecular gas. The high-precision positions determined in our work allow similar comparisons for a number of sources for which interferometric data of the molecular and ionized gas exist (see § 3). The clearest case is the bipolar outflow from the IRAS 20126+4104 HMC, where the 44 GHz masers are located very near the shocked gas as traced by H_2 and SiO emission in the flow (Fig. 19). Further evidence for the association of the 44 GHz line with shocked gas can be seen in G31.41+0.31 and G34.26+ 0.15 (Figs. 11 and 12), where the masers correlate very well with emission from the shock tracer SiO(2–1). Also, in DR 21(OH) (Fig. 21) the distribution and systematic shift of radial velocity strongly suggest an outflow origin for the 44 GHz masers. A detailed comparison of molecular shock tracers with the 44 GHz maser positions for all the sources in our sample is not possible owing to scarcity of interferometric outflow data and is beyond the scope of this work. Nevertheless, our data add a number of sources that strongly support the original hypothesis of Plambeck & Menten (1990). We note, however, that bipolar outflows might not be the only possible source of shocked gas that could give rise to class I methanol masers. In particular, accretion shocks very near the central object might also lead to the conditions for methanol masers. Possible candidates for this scenario are S235, Mol 136, Mol 138, and Mol 160, where the 44 GHz masers coincide with young stellar objects.

5. CONCLUSIONS

We have surveyed 44 massive star formation regions in the 7_0–6_1 A^+ methanol line, and report maser detections in 37 of these. Thirty-one of the 44 regions were also observed in the 9_2–10_1 A^+ methanol line, with two maser detections. Several possible explanations for the relatively low detection rate of 23 GHz masers are discussed. Thermal methanol emission was detected at 44 GHz toward G31.41+0.31 and at 23 GHz toward NGC 7538.

The median 5 σ detection limit is 0.2 Jy and typical astrometric precision is 0.″5. This is the most sensitive, highest angular resolution survey of 44 GHz masers made to date. We caution that the absolute flux density calibration is accurate only to the 20%–30% level, hence these data are not suitable for precise variability studies.

For a subsample of 22 fields containing both compact H II regions and 44 GHz maser emission, 86% of the masers are

within 0.5 pc projected distance from the ionized gas, with a median distance of 0.2 pc. This is distinctly smaller than the original class I/II classification scheme, which indicated 1–2 pc separations between class I masers and H II regions. This smaller separation, and also the good correlation of both 6.67 GHz and 44 GHz masers with compact H II regions in our sample, and the very low detection rate of 23 GHz masers, supports the suggestion of Slysh et al. (1994) that the class I/II definition is better based on transition than on association (or lack thereof) with other astronomical objects.

Several sources, most notably IRAS 20126+4104, G31.41+0.31, G34.26+0.15, and DR 21(OH) show evidence for a spatial correlation between the 44 GHz masers and shocked molecular gas, supporting the view that these masers may result from molecular outflows.

Sixteen fields show maser emission stronger than 10 Jy, and all of these should be excellent candidates for the maser cross-calibration technique, using the 44 GHz maser to calibrate 7 mm continuum or spectral line observations.

We thank D. Shepherd, Y. Gómez, and M. Sewilo for providing radio continuum images of several sources. S. K. acknowledges support from grant 36568-E, CONACyT, Mexico, and DGAPA, UNAM grant IN118401. P. H. acknowledges support from the Research Corporation award CC4996 and from NSF grant AST-0098524. We thank the anonymous referee for helpful suggestions that improved the quality of the paper. This research has made use of the SIMBAD database, operated at CDS, Strasbourg, France.

REFERENCES

Acord, J. M., Churchwell, E., & Wood, D. O. S. 1998, ApJ, 495, L107
Araya, E., Hofner, P., Churchwell, E., & Kurtz, S. 2002, ApJS, 138, 63
Bachiller, R., Menten, K. M., Gómez-González, J., & Barcia, A. 1990, A&A, 240, 116
Batrla, W., Matthews, H. E., Menten, K. M., & Walmsley, C. M. 1987, Nature, 326, 49
Bronfman, L., Nyman, L.-A., & May, J. 1996, A&AS, 115, 81
Campbell, M. F., Garland, C. A., Deutsch, L. K., Hora, J. L., Fazio, G. G., Dayal, A., & Hoffmann, W. F. 2000, ApJ, 536, 816
Campbell, B., & Thompson, R. I. 1984, ApJ, 279, 650
Cesaroni, R., Felli, M., Jenness, T., Neri, R., Olmi, L., Robberto, M., Testi, L., & Walmsley, C. M. 1999a, A&A, 345, 949
Cesaroni, R., Felli, M., Testi, L., Walmsley, C. M., & Olmi, L. 1997, A&A, 325, 725
Cesaroni, R., Felli, M., & Walmsley, C. M. 1999b, A&AS, 136, 333
Cesaroni, R., Olmi, L., Walmsley, C. M., Churchwell, E., & Hofner, P. 1994, ApJ, 435, L137
Churchwell, E. 2002, ARA&A, 40, 27
Churchwell, E., Walmsley, C. M., & Cesaroni, R. 1990, A&AS, 83, 119
Cragg, D. M., Sobolev, A. M., Caswell, J. L., Ellingsen, S. P., & Godfrey, P. D. 2004, MNRAS, 351, 1327
Downes, D., Wilson, T. L., Bieging, J., & Wink, J. 1980, A&AS, 40, 379
Evans, N. J. 1999, ARA&A, 37, 311
Evans, N. J., & Blair, G. N. 1981, ApJ, 246, 394
Felli, M., Massi, F., Navarrini, A., Neri, R., Cesaroni, R., & Jenness, T. 2004, A&A, 420, 553
Felli, M., Testi, L., Valdettaro, R., & Wang, J.-J. 1997, A&A, 320, 594
Fey, A. L., Claussen, M. J., Gaume, R. A., Nedoluha, G. E., & Johnston, K. J. 1992, AJ, 103, 234
Forster, J. R., & Caswell, J. L. 1989, A&A, 213, 339
Garay, G., & Lizano, S. 1999, PASP, 111, 1049
Garay, G., & Rodríguez, L. F. 1990, ApJ, 362, 191
Gaume, R. A., Fey, A. L., & Claussen, M. J. 1994, ApJ, 432, 648
Gaume, R. A., Goss, W. M., Dickel, H. R., Wilson, T. L., & Johnston, K. J. 1995, ApJ, 438, 776
Genzel, R., et al. 1981, ApJ, 247, 1039
Gómez, Y., Rodríguez, L. F., & Martí, J. 1995, ApJ, 453, 268
Haschick, A. D., Baan, W. A., & Menten, K. M. 1989, ApJ, 346, 330
Haschick, A. D., Menten, K., & Baan, W. A. 1990, ApJ, 354, 556
Hatchell, J., Fuller, G. A., & Millar, T. J. 2001, A&A, 372, 281
Heaton, B. D., Little, L. T., Yamashita, T., Davies, S. R., Cunningham, C. T., & Monteiro, T. S. 1993, A&A, 278, 238
Hofner, P., Cesaroni, R., Rodríguez, L. F., & Martí, J. 1999, A&A, 345, L43
Hofner, P., & Churchwell, E. 1996, A&AS, 120, 283 (HC96)
Hofner, P., Wiesemeyer, H., & Henning, T. 2001, ApJ, 549, 425
Hunter, D. A., & Massey, P. 1990, AJ, 99, 846
Johnston, K. J., Gaume, R., Stolovy, S., Wilson, T. L., Walmsley, C. M., & Menten, K. M. 1992, ApJ, 385, 232
Kogan, L., & Slysh, V. 1998, ApJ, 497, 800
Kurtz, S., Churchwell, E., & Wood, D. O. S. 1994, ApJS, 91, 659
Lo, K. Y., Burke, B. F., & Haschick, A. D. 1975, ApJ, 202, 81
Mangum, J. G., Wootten, A., & Mundy, L. G. 1992, ApJ, 388, 467
Maxia, C., Testi, L., Cesaroni, R., & Walmsley, C. M. 2001, A&A, 371, 287
Menten, K. 1991, in ASP Conf. Ser. 16, Atoms, Ions and Molecules: New Results in Spectral Line Astrophysics, ed. A. D. Haschick & P. T. P. Ho (San Francisco: ASP), 119
Menten, K. M., & Batrla, W. 1989, ApJ, 341, L91
Menten, K. M., Johnston, K. J., Wadiak, E. J., Walmsley, C. M., & Wilson, T. L. 1988, ApJ, 331, L41
Molinari, S., Brand, J., Cesaroni, R., & Palla, F. 1996, A&A, 308, 573
———. 2000, A&A, 355, 617
Molinari, S., Brand, J., Cesaroni, R., Palla, F., & Palumbo, G. G. C. 1998, A&A, 336, 339
Molinari, S., Testi, L., Rodríguez, L. F., & Zhang, Q. 2002, ApJ, 570, 758
Olmi, L., Cesaroni, R., Neri, R., & Walmsley, C. M. 1996a, A&A, 315, 565
Olmi, L., Cesaroni, R., & Walmsley, C. M. 1996b, A&A, 307, 599
Pestalozzi, M. R., Elitzur, M., Conway, J. E., & Booth, R. S. 2004, ApJ, 603, L113
Plambeck, R. L., & Menten, K. M. 1990, ApJ, 364, 555
Pratap, P., Megeath, S. T., & Bergin, E. A. 1999, ApJ, 517, 799
Reid, M. J., & Menten, K. M. 1990, ApJ, 360, L51
Reifenstein, E. C., Wilson, T. L., Burke, B. F., Mezger, P. G., & Altenhoff, W. J. 1970, A&A, 4, 357
Roelfsema, P. R., Goss, W. M., & Geballe, T. R. 1989, A&A, 222, 247
Sewilo, M., Churchwell, E., Kurtz, S., Goss, W. M., & Hofner, P. 2004, ApJ, 605, 285
Shepherd, D. S., Testi, L., & Stark, D. P. 2003, ApJ, 584, 882
Shepherd, D. S., Yu, K. C., Bally, J., & Testi, L. 2000, ApJ, 535, 833
Slysh, V. I., Kalenskii, S. V., Val'tts, I. E., & Otrupcek, R. 1994, MNRAS, 268, 464
Testi, L., Hofner, P., Kurtz, S., & Rupen, M. 2000, A&A, 359, L5
Tofani, G., Felli, M., Taylor, G. B., & Hunter, T. 1995, A&AS, 112, 299
Torrelles, J. M., Gómez, J. F., Rodríguez, L. F., Ho, P. T. P., Curiel, S., & Vázquez, R. 1997, ApJ, 489, 744
Walsh, A. J., Burton, M. G., Hyland, A. R., & Robinson, G. 1998, MNRAS, 301, 640
Walsh, A. J., Macdonald, G. H., Alvey, N. D. S., Burton, M. G., & Lee, J.-K. 2003, A&A, 410, 597
Wilking, B., Mundy, L., McMullin, J., Hezel, T., & Keene, J. 1993, AJ, 106, 250
Wood, D. O. S., & Churchwell, E. 1989, ApJS, 69, 831 (WC89)
Zheng, X. W., Ho, P. T. P., Reid, M. J., & Schneps, M. H. 1985, ApJ, 293, 522